Mechanical, durability, depolluting and electrical properties of multifunctional mortars prepared with commercial or waste carbon-based fillers

Alessandra Mobili[1], Alberto Belli[2], Chiara Giosuè[1], Mattia Pierpaoli[3], Luca Bastianelli[4], Alida Mazzoli[1], Maria Letizia Ruello[1], Tiziano Bellezze[1], Francesca Tittarelli[1,5]

[1]*Department of Materials, Environmental Sciences and Urban Planning (SIMAU), Università Politecnica delle Marche, via Brecce Bianche 12, 60131, Ancona, Italy –INSTM Research Unit.*

[2]*Department of Applied Science and Technology (DISAT), Politecnico di Torino, INSTM Research Unit, Corso Duca degli Abruzzi 24, 10129, Torino, Italy*

[3]*Department of Metrology and Optoelectronics, Faculty of Electronics, Telecommunication and Informatics, Gdansk University of Technology, 80-233 Gdansk, Poland*

[4]*Department of Information Engineering (DII), Università Politecnica delle Marche, via Brecce Bianche 12, 60131, Ancona, Italy.*

[5]*ISAC – CNR, via Piero Gobetti 101, 40129, Bologna, Italy.*

Corresponding author: Tel.: +39 071 2204726.

E-mail address: a.mobili@univpm.it (A. Mobili).

Highlights

- Commercial and waste carbon-based fillers are compared in lime-based mixes
- Waste fillers increase the compressive strength of lime-based mixes
- Waste fillers decrease lime-based mixes water suction and increase VOCs adsorption
- Waste fillers increase electrical conductivity and EMI SE of lime-based mixes
- Waste fillers are a sustainable and cheap alternative for multifunctional mixes

Abstract

Carbon-based fillers from industrial wastes and commercial ones were compared to improve the properties of lime-based mixes. As commercial fillers, graphene nanoplatelets and activated carbon were used, whereas as industrial wastes a char obtained by the gasification of biomasses and a used foundry sand were chosen. Carbon-based wastes were found to be a good cost-effective alternative to commercial carbon based fillers to increase the compressive strength (of about 25%) and to reduce water capillary absorption (of about 50%) thanks to the paste refinement; to enhance depollution capacity (of about 25%) and increase both electrical conductivity (up to 65%) and electromagnetic shielding effectiveness (of about 6%) of the hardened compounds thanks to the carbon content.

Keywords

Mortar, Multifunctionality, Carbon-based filler, Mechanical properties, Durability, Depollution, Electrical properties.

1. Introduction

In the last two decades, carbon-based commercial fillers as carbon black, graphene and its derivatives (carbon nanotubes, fullerenes, etc.), and carbon nanofibers have been studied as possible additions in binder-based matrices in order to improve their multifunctionality. As a matter of fact, thanks to their high mechanical strength, high specific surface area, porosity, lightness, and high electrical conductivity [1,2] they can enhance the mechanical, durability, depolluting and especially electrical and electromagnetic properties of mortars and concretes [3–7].

In particular, air pollution, related to the dispersion in atmosphere of particulate matters (PMs), nitrogen oxides (NO_x), and volatile organic compounds (VOCs), is a serious problem not only for outdoor but also for indoor environments where respiratory diseases and the so-called “Sick Building Syndrome” can affect the health of occupants [8] since people spend about 90% of their time in confined environments [9]. Also electromagnetic (EM) radiations generated by electronic devices and communication systems, particularly at high frequencies, can be dangerous for humans [10,11], besides interfering with other electronic devices [12–14].

A possible solution to these issues can be the development of multifunctional building materials that can both decrease the concentration of air pollutants and reduce the spreading of EM signals in confined environments. Indeed, considering air depollution, up to now, several indoor air cleaning technologies have been improved; not only active technologies, which are energy consuming, as filtration, non-thermal plasma and electrostatic precipitator [15] but also more sustainable passive technologies, that can interact with the active technologies minimizing the energy consumption, using construction materials as substrates for adsorption and photocatalysis have been developed. In particular, adsorption can occur on highly porous materials, with high specific surface area (300-3000 m^2/g) [16], and photocatalysis can mineralize pollutants into less harmful compounds by means of a nano-catalyst, such as titanium dioxide (TiO_2) activated under UV-A radiation [17]. Construction materials can also reduce passively the spreading of EM signals if, again, a high specific surface area with porous materials is guaranteed since it enhances the electromagnetic shielding property [18] of materials, that is the property to reflect and/or absorb electromagnetic radiations.

So far, carbonaceous fillers addition has been extensively studied in binder-based materials.

Activated carbon is one of the most efficient adsorptive materials for gases and vapours (VOCs or NO_x) in air or pollutants in water both if used as it is [19,20] or if it is dispersed within a matrix [21,22]. The effectiveness depends on its wide surface area, porosity and chemical functional group that can act even in a binding matrix. Researchers have been also studied low-cost alternatives such as from waste precursor [23]. Activated carbon, can also enhance the electromagnetic shielding effectiveness of construction materials through the multiple reflections phenomenon [24].

Graphene and its derivatives, because of their high specific surface area, are suitable for gas sorption materials [25]. Le et al. [2] proved that GNP is able to enhance the electrical conductivity of cement-based composites and if GNP content exceeds the percolation value (the limit beyond which the conductive particles touch each other), the moisture content does not influence the electrical conductivity. Liu et al. [26] reported that GNP is better than graphene oxide nanoplatelets (GONP) to manufacture electrically conductive cement-based materials. Moreover, GNP is reported to be suitable also to produce mortars with piezoresistive behaviour [27,28], thus the material changes its electrical resistivity if subjected to strain [29,30].

However, the essential prerequisite for the efficient use of carbon-based fillers to enhance multi-functionality of binder-based composites is their good dispersion in the mix. Unfortunately, carbon-based commercial fillers can be barely dispersible in polar liquids like water, since, due to their high specific surface area, Van der Waals' forces create bundles and agglomerates. Moreover, many commercial carbon-based materials as graphene nanoplatelets (GNP) and carbon nanotubes are highly expensive and some of them, as carbon black or carbon nanotubes, are very toxic [31,32].

Cost can be saved by using carbon-based industrial by-products obtained by the thermal treatment of biomasses that are much cheaper, being wastes, than commercial ones. Moreover, thanks to a different chemical composition with the presence of functional groups formed by other elements than carbon (as Mg, Al, Ca, Si, Na, K, Fe, O), they result more compatible with water and then easily dispersible in polar liquids [33].

Char is an industrial by-product obtained by treating biomasses at high temperatures, as in the gasification process. Gasification takes place at T = 500-1400 °C and the resulting char is a highly porous material mainly composed by carbon [34]. A recent paper by Sirico et al. [35] reports that the addition of char from gasification to mortars at 1 wt.% by cement maintains both the compressive and flexural strengths similar to those of control specimens by slightly increasing the fracture energy. Some studies have confirmed that thermal treated biomasses or waste biomass ashes can enhance the absorption of VOCs [36,37] and can be a potential low-cost substitutes of activated carbon for air depollution [34]. Moreover, the high carbon content makes char a good candidate also for enhancing the electromagnetic shielding effectiveness and electrical properties of construction materials.

Used foundry sand is another industrial by-product obtained by the ferrous and non-ferrous metal casting industries where it is used as a moulding casting material because of its great thermal conductivity. The addition of used foundry sand has been already studied in cement-based mortars/concretes; however, its use has been mainly focused as substitute of natural sand [38,39]. Used foundry sand has a high silica content, but contains also carbonaceous additions and several metals [40]. Also in this case, the carbonaceous additions and the elevated metal content make this by-product a good candidate to enhance the electromagnetic shielding effectiveness and electrical properties of construction materials.

Therefore, in this paper, two commercial carbon-based fillers, graphene nanoplatelets and powdered activated carbon, and two different low cost waste carbonaceous fillers, a char from gasification of biomasses and the finest fraction of a used foundry sand, have been compared as addition to enhance the mechanical, durability, depolluting, and electrical properties of pastes/mortars. As binder, a hydraulic lime was chosen, since lime-based mortars are extensively used as renders/panels in indoor applications. Moreover, hydraulic lime mortars are commonly used for rehabilitation of historical buildings due to their compatibility with the substrate, where instead cement-based mortars are not allowed, and lime is a more sustainable binder than ordinary Portland cement [41]. Literature reports only few articles on the effect of carbon-based fillers on the properties of lime-based mortars: graphene oxide added at 0.05 and 0.1 wt.% by lime [42] and the replacement of lime with waste graphite powder up to 25 wt.% [43] are able to increase the mechanical performance of mortars by decreasing their porosity. A recent paper published by some of the present authors has focused on the use of gasification char and used foundry sand at 1.0% on the total volume as alternatives to graphene nanoplatelets to decrease the electrical resistivity of cement-based mortars [44]. In the paper, it was found that gasification char is better than used foundry sand to enhance some properties of cement mortars since it decreases by 42% their electrical resistivity and by 17% their capillary water absorption. However, to the best of authors' knowledge, there are no paper dealing with the use of gasification char and used foundry sand as carbonaceous by-products for enhancing properties of hydraulic lime-based mixes. Moreover, in the present paper lime-based pastes have been subjected to investigation, to enhance the effect of additions on the matrix since, as reported in [45], aggregates can act as an obstacle in the electric current path increasing the electrical resistivity of concrete.

2. Experimental

2.1 Materials

Natural hydraulic lime (NHL 5, according to UNI EN 459-1) was used as binder.

As commercial carbon-based fillers, graphene nanoplatelets (GNP) (Pentagraf, Pentachem S.r.l.), with a thickness of 6 – 8 nm and a width lower than 5 µm and activated carbon (AC) (Norit® CAP SUPER-WJ, Cabot Norit Nederland B.V.) with a mean particle size of 20 µm were used. GNP has a BET surface area of 30 m^2/g, whereas AC has a BET surface area of 1800 m^2/g.

As waste fillers, a char (CH) from biomasses gasification, provided by a plant located in central Italy, and the finest fraction of a used foundry sand (FS), provided by the Italian company LA.BO S.r.l. were used. In particular, CH is obtained by the gasification (Holz-Kraft, Spanner Re² GmbH gasifier) of natural wood chips, after to be dried to a moisture content lower than 13%. CH and FS were ground and sieved in order to have a particle size distribution lower than 75 µm. CH and FS have a BET surface area of 76 m^2/g and 341 m^2/g, respectively. The full characteristics of CH and FS are reported in [44].

The morphology of the fillers analysed by Scanning Electron Microscopy (SEM) and the corresponding elemental analysis obtained by EDX-Analysis are given in Fig. 1 and Table 1, respectively. The SEM images highlight the flat shape of GNP (Fig. 1a), the spherical shape of FS (Fig. 1d) and the more elongated aspect of both AC and CH fillers (Figs. 1b and 1c, respectively).

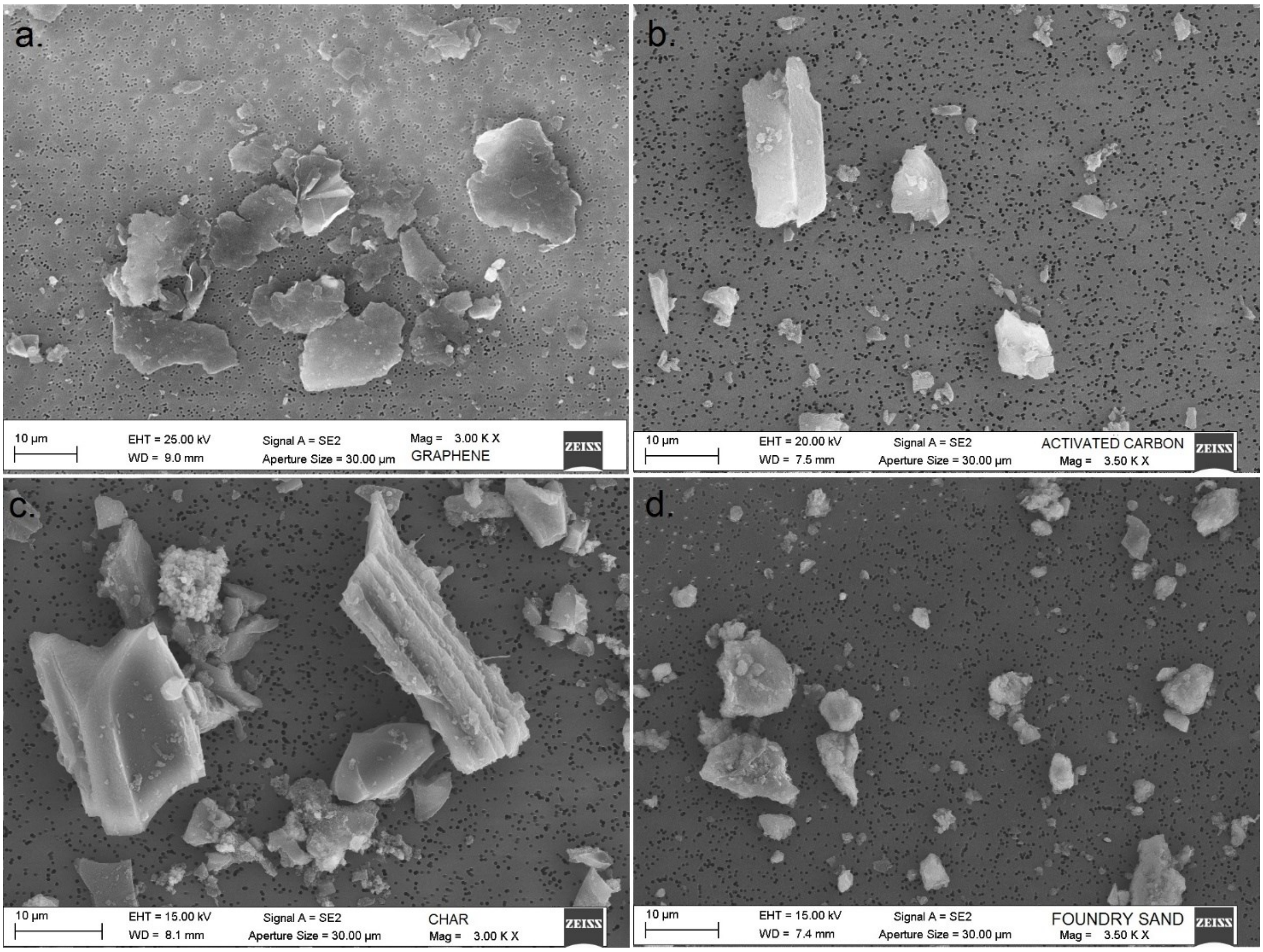

Fig. 1. SEM of carbonaceous fillers: a. graphene nanoplatelets (GNP); b. activated carbon (AC); c. char (CH) from gasification minor of 75 µm; d. foundry sand (FS) minor of 75 µm.

Table 1. Elemental analysis of waste carbonaceous fillers (wt.%).

Filler	C	O	Ca	K	Mg	Si	Al	Na	Fe
GNP	99.50	0.50	-	-	-	-	-	-	-
AC	95.23	4.77	-	-	-	-	-	-	-
CH	76.72	14.93	5.39	2.04	0.57	0.36	-	-	-
FS	32.92	37.87	1.91	0.66	1.18	14.83	6.38	1.97	2.28

SEM and ImageJ processing software have been used to evaluate the morphology of the particles and to measure both the particle size and size distribution of AC and CH. An image analysis method was conducted, since indirect advanced methods (e.g. those involving scattered, diffracted light or laser) assume the particle being spherical, which was not the predominant case of AC and CH (Figs. 1b and 1c). In fact, for those particles that show an irregular shape, assuming them to be regular and geometrical will result in an oversimplification. The irregular particles have been described by the diameter of a circle of equal projection area (d_{EC}), Feret's diameter (d_F) and minimal Feret's diameter ($Min\ d_F$), on the basis of previous researches carried out by the authors [46,47].

Table 2. Mean values and standard deviations of d_{EC}, d_F and $Min\ d_F$ for CH and AC samples.

Sample	d_{EC} (μm)	d_F (μm)	$Min\ d_F$ (μm)
CH	1.6 ± 2.5	2.5 ± 3.5	1.5 ± 2.3
AC	2.8 ± 3.2	4.7 ± 4.5	2.9 ± 3.0

In the case of GNP and FS, the particle size distribution was determined by laser diffraction analysis, since both showed a predominant spherical morphology (Figs. 1a and 1d). Results are showed in Fig. 2: FS sieved at 75 μm is finer than GNP, which shows also a broader grain size distribution.

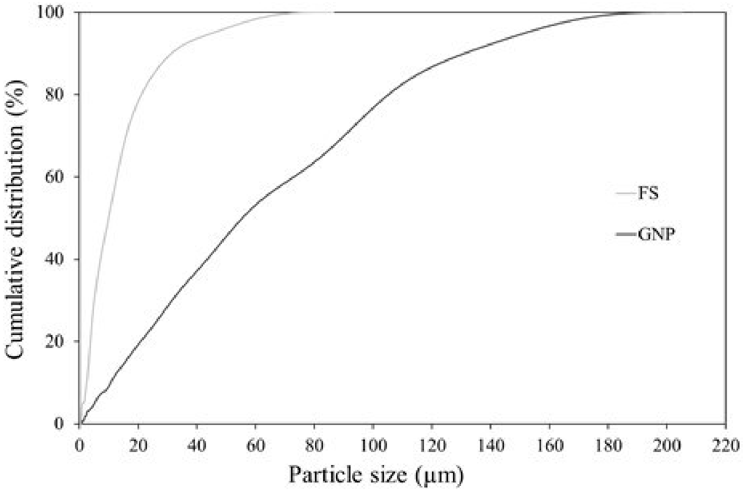

Fig. 2. Particle size distribution of graphene nanoplatelets (GNP) and foundry sand (FS) with particle size distribution lower than 75 μm.

2.2 Preparation of the dispersion

To better disperse each carbonaceous addition, fillers were put into different solutions, composed by water or by water and superplasticiser. Three different samples were prepared: one containing water and GNP and two containing water, superplasticiser and GNP. Two types of liquid superplasticiser were compared: a naphthalene sulphonate superplasticiser (N200) (Mapefluid N200, Mapei S.p.A.) and an acrylic superplasticiser (SP1) (Dynamon SP1, Mapei S.p.A.). N200 and SP1 were added in two different amounts, namely 0.5 wt.% and 1.0 wt.% of the binder, whereas GNP was added at 0.5 wt.% of the binder. Initially, the compounds were manually stirred for 1 minute; then, they underwent to sonication with an ultrasonicator for 10 minutes at 20 °C (the complete characteristics of the ultrasonicator are reported below). The quality and stability of the dispersions were evaluated by means of a portable turbidimeter (Orbeco-Hellige Model 966) after set periods of time, namely immediately after sonication and after 5, 15, 30, 60 and 120 minutes. Also the amount and type of superplasticiser for preparing the final mixtures were chosen after the evaluation of GNP dispersion by means of the turbidimeter. The turbidimeter works with a light beam which passes through the sample, if there are suspended particles the light is scattered. The dispersions were evaluated in terms of turbidity, which describes the cloudiness of a fluid caused by large numbers of individual particles, generally invisible to the naked eye. The turbidity is measured by Nephelometric Turbidity Units (NTU); if a substance is completely dissolved in solution, light is nearly no scattered leading to a low NTU value, whereas if the solubility limit is reached and the substance starts to precipitate, the light is strongly scattered leading to a high NTU value.

When SP1 and N200 were added to 0.5 wt.% of the binder, the NTU values after sonication were 1.30 and 1.00, whereas after 5 minutes 2.00 and 1.40, respectively. On the other hand, when SP1 and N200 were added to 1.0 wt.% of the binder, after sonication the NTU values were 0.16 and 0.11, whereas after 5 minutes 0.18 and 0.16, respectively. The slightly lower NTU values obtained by samples prepared with N200 compared to those containing SP1 mean that N200 is better than SP1 to disperse GNP. Moreover, when the superplasticiser is added at 1.0 wt.%, the dispersion is more homogeneous than when added at 0.5 wt.%; for this reason, it was decided to use the superplasticiser at 1.0 wt.% on the binder.

The turbidity levels of the dispersions prepared with the sole water and with 1.0 wt.% of superplasticisers in time are reported in Fig. 3. Immediately after sonication, the dispersion of GNP prepared with N200 obtained a lower NTU value compared to that prepared with SP1. This condition is maintained for the first 30 minutes after sonication, whereas later the two curves invert (Fig. 3a) and SP1 becomes the one which ensures the best dispersion up to 2 hours of sonication (Fig. 3b). On the other hand, when water alone is used as dispersant (H2O curve), the dispersion has a much higher NTU value, which is maintained for all the duration of the test (Fig. 3b), meaning that water alone is not effective neither to disperse GNP nor to maintain the dispersion stable after sonication.

After a short period of time (30 minutes), the addition of N200 to water ensured a better dispersion of GNP compared to SP1. This is in agreement with other studies which suggest the use of naphthalene sulphonate superplasticiser as dispersing agent for carbonaceous fillers [2,48,49].

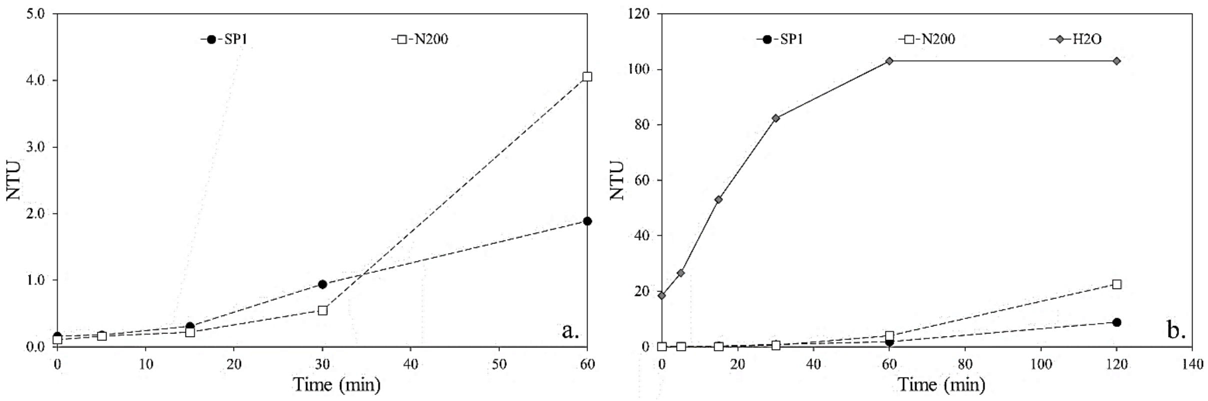

Fig. 3. Turbidity of the dispersion evaluated in terms of Nephelometric Turbidity Units (NTU) after a. 60 mins after sonication (enlargement) and b. 120 mins after sonication.

2.3 Preparation of specimens

The pastes were manufactured in order to reach a stiff consistency (flow value ≤ 140 mm, UNI EN 1015:3), by using N200 and different amounts of carbonaceous fillers (0.25, 0.50 and 1.00 wt.% on lime). As reference (REF), a paste without filler addition was prepared. Mix proportions and workability of pastes are reported in Table 3.

Table 3. Mix proportions and flow values of pastes submitted to mechanical, microstructural, capillary water absorption, electrical conductivity and depolluting tests (flow and in batch tests).

Mixtures	NHL 5 (g/L)	Water (g/L)	N200 (g/L)	GNP (g/L)	AC (g/L)	CH (g/L)	FS (g/L)	w/b	Flow value (mm)
REF	1375	441	13.75	-	-	-	-	0.32	117
GNP 0.25	1375	441	13.75	3.44	-	-	-	0.32	112
GNP 0.50	1375	441	13.75	6.87	-	-	-	0.32	112
GNP 1.00	1375	441	13.75	13.75	-	-	-	0.32	107
AC 0.25	1375	441	13.75	-	3.44	-	-	0.32	112
AC 0.50	1375	441	13.75	-	6.87	-	-	0.32	107
AC 1.00	1375	456	13.75	-	13.75	-	-	0.33	107
CH 0.25	1375	441	13.75	-	-	3.44	-	0.32	109
CH 0.50	1375	441	13.75	-	-	6.87	-	0.32	113
CH 1.00	1375	441	13.75	-	-	13.75	-	0.32	110
FS 0.25	1375	441	13.75	-	-	-	3.44	0.32	112
FS 0.50	1375	441	13.75	-	-	-	6.87	0.32	115
FS 1.00	1375	441	13.75	-	-	-	13.75	0.32	112

In order to analyse the effect of carbonaceous fillers on the depolluting activity in terms of NO_x abatement, pastes were also prepared by adding 1 wt.% on lime of a titanium dioxide photocatalytic agent (TiO_2), AEROXIDE® TiO_2 P 25 (Evonik Resource Efficiency GmbH). In fact, its photocatalytic activity under UV radiation is a well-known issue [6]. Pastes compositions with TiO_2 addition are reported in Table 4.

Table 4. Mix proportions of pastes with TiO_2 submitted to depolluting tests (flow test).

Mixtures	NHL 5 (g/L)	Water (g/L)	N200 (g/L)	GNP (g/L)	AC (g/L)	CH (g/L)	FS (g/L)	TiO_2 (g/L)	w/b
REF T	1434	545	14.34	-	-	-	-	14.34	0.39
GNP 0.50 T	1434	545	14.34	7.17	-	-	-	14.34	0.39
AC 0.50 T	1434	545	14.34	-	7.17	-	-	14.34	0.39
CH 0.50 T	1434	545	14.34	-	-	7.17	-	14.34	0.39
FS 0.50 T	1434	545	14.34	-	-	-	7.17	14.34	0.39

The electromagnetic shielding effectiveness was evaluated on mortars prepared with a water/binder (w/b) ratio of 0.49 and a calcareous sand with a maximum grain size of 3 mm (sand/lime ratio = 3 wt.%). In order to prevent detachment or cracking of mortars due to shrinkage from the sample holder used in SE measurements, a shrinkage reducing admixture (SRA) (Mapecure SRA, Mapei S.p.A.) and a CaO expansive agent (Expancrete, Mapei S.p.A.) in amounts equal to 2 and 5 wt.% on lime, respectively, were added to mortars. Carbon-based fillers were added at the same dosage weight of dry materials used for pastes, namely 0.50 wt.% on lime for GNP and AC and 1.00 wt.% on lime for CH and FS, respectively. The fillers dispersion was carried out with the same procedure used for pastes. Mortars compositions are reported in Table 5.

Table 5. Mix proportions of mortars submitted to electromagnetic shielding property tests.

Mixtures	NHL 5 (g/L)	Water (g/L)	N200 (g/L)	GNP (g/L)	AC (g/L)	CH (g/L)	FS (g/L)	SAND (g/L)	CaO (g/L)	SRA (g/L)	w/b
M REF	524	256	13.75	-	-	-	-	1611	26.19	10.47	0.49
M GNP 0.50	524	256	13.75	6.87	-	-	-	1611	26.19	10.47	0.49
M AC 0.50	524	256	13.75	-	6.87	-	-	1611	26.19	10.47	0.49
M CH 1.00	524	256	13.75	-	-	13.75	-	1611	26.19	10.47	0.49
M FS 1.00	524	256	13.75	-	-	-	13.75	1611	26.19	10.47	0.49

Pastes were prepared by mixing the blend of water, N200 and filler with the lime (previously mixed with TiO_2, if necessary) until homogeneity for 3 minutes.

To manufacture mortars, lime was previously mixed with CaO and sand until homogeneity was reached, and then the blend of water, superplasticiser and filler was incorporated. Finally, SRA was added to the mortar and mixed for 3 minutes.

Superplasticiser was manually stirred together with the mixing water, later the carbonaceous fillers were added to the liquid. Fillers were dispersed for 10 minutes at 20 °C by means of an ultrasonicator Vibra Cell^{TM} VCX 130 (Sonics & Materials, Inc.) equipped with a probe with a diameter of 13 mm that works with a frequency of 20 kHz by setting an amplitude of 70%. Since the stability of the dispersion with N200 is ensured during the first 30 minutes after sonication (Fig. 3a), the dispersion was immediately mixed with dry materials for the preparation of pastes and mortars in order to avoid a possible sedimentation of the carbon-based fillers.

After mixing, the workability of pastes was measured in accordance with the UNI EN 1015-3 standard.

Pastes and mortars were poured into different moulds according to the tests to be carried out and cured at T = 20 ± 1 °C and RH = 95 ± 5% for 7 days and then maintained at T = 20 ± 1 °C and RH = 50 ± 5% until testing.

2.3 Methods

2.3.1 Mechanical characterization

In order to investigate the effect of the fillers on the mechanical properties of the pastes (Table 3), three specimens with 40x40x160 mm dimensions were manufactured and submitted to both compression and tensile splitting tests after 2, 7 and 28 days of curing according to UNI EN 1015-11 and UNI EN 12390-6, respectively.

2.3.2 Microstructural characterization

To establish the correlation of the obtained results with the microstructure, mercury intrusion porosimetry (MIP) was performed using a Thermo Fisher Pascal 240 porosimeter to analyse the pore size distribution and the total open porosity (V_p) of pastes. One small fragment for each composition (Table 3) of about 1 cm^3 was tested after 28 days of curing. Moreover, SEM observations were performed using a SEM PHILIPS XL20 equipment on small samples of graphite coated paste specimens (Table 3) after 28 days of curing.

2.3.3 Capillary water absorption

Since water is the medium and the main carrier of aggressive ions (Cl^-, SO_4^{2-}, etc.) [50,51], the study concerning the water absorption is of primary importance to give information on the durability of a construction material. The durability of pastes (Table 3) was studied through capillary water absorption tests by measuring the amount of water absorbed by a dried specimen through capillary suction in time. For short contact periods (90 min), the capillary water absorption coefficient (*C*) was calculated on three 40x40x80 mm paste specimens per composition according to UNI EN 1015-18 and the average result was reported. For long contact periods, the water absorbed per unit area (Q_i) by the same three specimens per compositions was measured for 8 days according to UNI EN 15801.

2.3.4. Depolluting Tests

In order to investigate if the carbonaceous fillers additions used in this research could give a certain depolluting activity to lime-based materials, the depolluting properties of different pastes were evaluated after 28 days of curing. Two different experimental tests were performed: in-batch, in order to explore the effect of different fillers on the adsorbent properties of pastes for VOCs; and in continuous, by flow test method inside a reactor, to highlight the possible effect of the carbon-based fillers on the photocatalytic ability of pastes. In flow test, pastes with and without TiO_2 were characterized (Table 4 and Table 3, respectively).

2.3.4.1. In batch test

In batch test Gas Chromatography was used for monitoring the concentration of Methyl-ethyl-ketone (MEK) against time injected in a 16.65 L sealed glass box containing the tested specimen [52]. Inside the box a fan guaranteed a continuous air recirculation. The specimens were cylinders with an exposed area of 5026 mm^2. For each composition, one specimen was tested. Air samples inside the box were collected by a micro-syringe every 8 min and analysed with a gas chromatograph (GC 8000 Top Carlo Erba instruments®, injector split 1:15, carrier control by flow; capillary column characteristics: length 25 m, thickness 0.52 µm, Ø 0.32 mm, crosslinked Methyl Siloxane, isotherm 50 °C, FID Detector). The initial amount of MEK injected into the test box was 50 µL which corresponds to 2402 mg/m^3 (approximately four times the Threshold Limit Value – TLV). The monitoring over time of data started after 20 min from the first injection to guarantee that all MEK was vaporised. Then, the results were plotted as a percentage of the concentration detected (C_i) with respect to the initial concentration (C_0). The tests were conducted in dark condition (absence of irradiation) for 110 minutes.

2.3.4.2. Flow test

The continuous flow test was performed according to UNI 11247 [8]. The specimens, with the same dimensions of those used for the in batch test, were placed on a tripod inside a borosilicate glass chamber of 3.58 L. An UVA metal-halogen quartz lamp (power 400 W), with mercury vapour peak at 360 nm irradiated the specimen surface. The distance between the surface of the specimen and the lamp guarantees a specimen radiance of about 20 W/m^2 , measured before each test [8]. The inlet gas was a mixture of synthetic air and NO_x. The chamber was linked to an analyser Monitor Labs, Nitrogen Oxides Analyser model 8841. The guaranteed inlet concentration of NO_x was 500 ppb and the abatement coefficient A_c (the percentage of NO_x abated) was evaluated according to UNI 11247.

2.3.5. Electrical and electromagnetic shielding properties

Finally, the electrical and electromagnetic shielding properties of mortars were tested. It is well-known that electrical and electromagnetic properties are related, and generally, at the lowest electrical resistances, the best results for electromagnetic SE are found [53–55].

2.3.5.1. Electrical resistivity

The electrical resistivity of a material can be measured by using alternating current (AC) [56] or direct current (DC) [28]. In this paper, electrical resistivity (ρ) was determined by means of a DC four-probe approach (Fig. 4) on three paste specimens per composition (Table 3) at 7, 14, 21 and 28 days of curing. The four-probe approach was used to determine the potential difference across the specimens, after the application of a set constant current, and to remove the effects of electrodes polarization. During casting, two AISI 304 stainless steel sheets (30x50x1 mm) were immersed in each specimen, 30 mm depth, leaving out the remaining 20 mm on the top of the surface and at a distance of 120 mm each one (Fig. 4). At the same way, two AISI 304 stainless steel rods (Ø 3 mm) were immersed in the specimens, 20 mm depth and placed at 100 mm each one, 10 mm far from the corresponding sheet at the same specimen side, as showed in Fig. 4. A constant DC current was applied by an Amel Mod. 2059 potentiostat/galvanostat on the outer two stainless steel sheets, and the potential difference was measured using a high impedance digital multimeter between the inner two stainless steel rods.

Since each electrolytic cell, as the lime pastes, is characterized by its own specific geometry, a cell-constant *K* must be determined for it, considering that this particular conductor is conforming to the second Ohm's Law:

$$R=\rho\frac{l}{A} \tag{1}$$

where *R* (Ω) is the resistance of the electrolytic conductor into the cell, measured between two hypothetic metallic electrodes, placed at a distance of *l* cm and having a contact area *A* (cm^2). The cell-constant *K* is given by the *l/A* ratio (cm^{-1}), whereas ρ ($\Omega\cdot cm$) is the resistivity of the electrolytic conductor and the inverse ($1/\rho$) its conductivity κ ($\Omega^{-1}\cdot cm^{-1}$ or $S\cdot cm^{-1}$; S = siemens). Considering that an ideal cell, with well-defined geometrical dimensions, does not exist, for real cells as showed in Fig. 4, *K* was determined by the immersion of the four-probes in an aqueous solution having a known *K* value, at the same configuration showed in Figure 4. Therefore, using the same equipment described above, the resistance *R* was measured and κ was calculated using the Eq. (1). The solution used for this purpose was KCl 0.01 M, having κ = 1.408 $mS\cdot cm^{-1}$ at 25 °C [57]. Actually, the conductivity of this solution was experimentally measured with an electrical conductivity meter AMEL Mod. 160 and the value κ = 1.442 $mS\cdot cm^{-1}$ was obtained.

In detail, in order to obtain the value of the resistance *R* of the cell with KCl solution for all the specimens, firstly, the potential difference (ΔV_0) between the two rods was measured in absence of current, then, a constant current *I* was applied between the two sheets in the range 5 – 10000 µA and the new potential difference (ΔV_i) was measured. These measurements were plotted in a (ΔV_i - ΔV_0) vs *I* diagram (Fig. 5). Interpolating the values that showed a linear trend, the value of the electrical resistance R was obtained. From this R value, a cell-constant $K = 0.6849\ \text{cm}^{-1}$ was calculated. Using Eq. (1) and this K value, from R determinations, ρ values were calculated for all specimens as a function of the curing time.

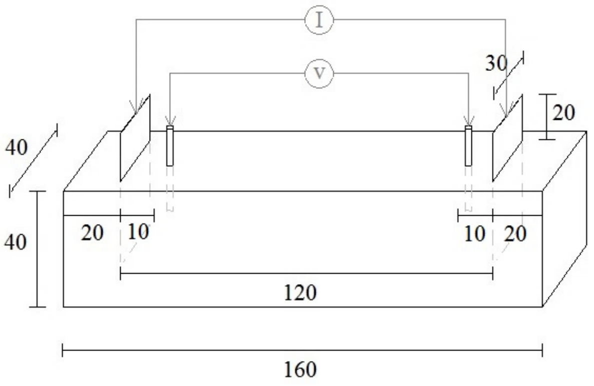

Fig. 4. Specimen scheme and electrodes configuration for DC electrical resistivity measurements.

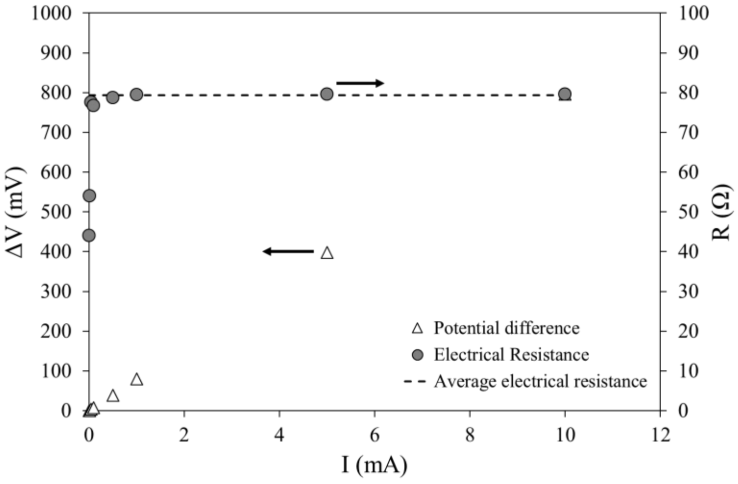

Fig. 5. Example of the determination of the electrical resistance (R) through potential difference ($\Delta V_i - \Delta V_0$) and current (I) measurements.

2.3.5.2. Electromagnetic shielding property

The electromagnetic shielding properties of the materials can be evaluated in diverse ways. In this paper the use of a reverberation chamber (RC) was proposed. The RC facility is able to reproduce a real environment, where the electromagnetic field is statistically uniform, isotropic and with random polarization [58]. In this way, the sample was excited from all the possible directions (polarization and incident angle), as a real-life scenario. In order to evaluate the SE, a smaller chamber with an aperture, called nested chamber, was used. The sample under test (Table 5) was mounted on the aperture [59,60]. Fig. 5a shows the adopted measurement setup. The outer RC which excites the material under test had dimensions of 6x4x2.5 m^3, whereas the inner chamber of 1.2x0.9x0.8 m^3. Within the outer RC, vertical and horizontal stirrers made of metallic rotating paddles provided the field mixing. The sample was placed on the aperture (Fig. 5b). In order to have an optimal contact between the sample edges and the aperture perimeter, avoiding field leakages [61], electromagnetic gaskets was used (Fig. 5b). Moreover, in order to improve the contact between the sample and the aperture, a multi-hole frame (Fig. 5c) with screws, pushing the sample towards the underlying gaskets, was used (Fig. 5d).

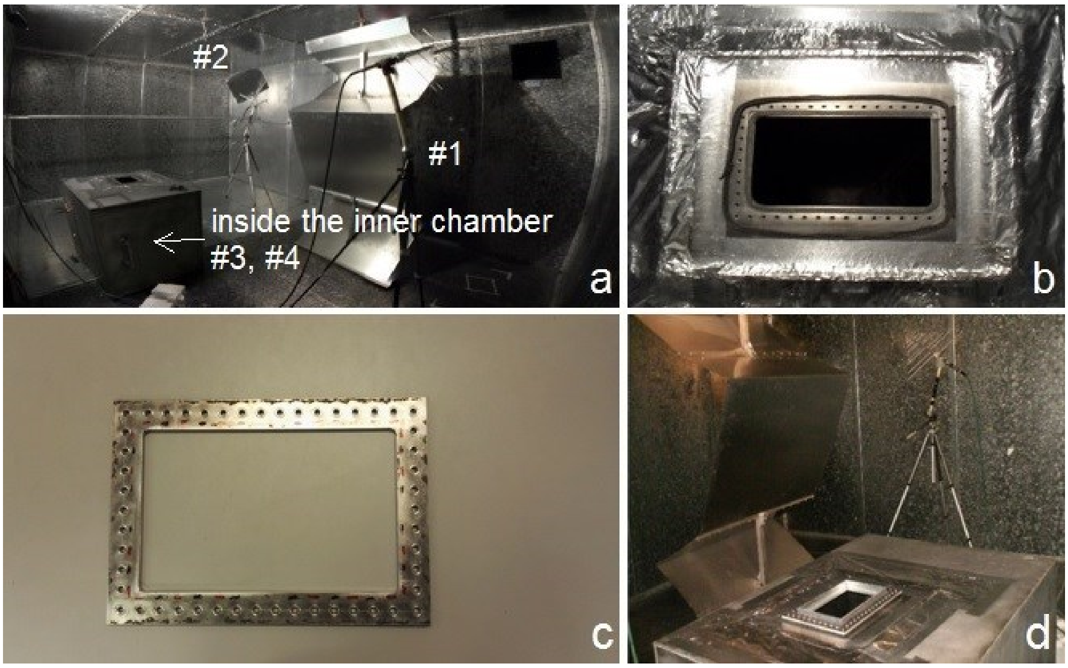

Fig. 5. a) Measurement set-up: outer RC equipped by vertical and horizontal stirrers, two log-periodic antennas and nested RC with the aperture on the top; b) aperture of the nested RC where both the gaskets used to avoid field leakages and the holes, where the multi-hole frame was mounted with screws to fasten the specimens and to provide a good contact, are visible; c) multi hole frame used to

improve the mechanical contact between the sample and the aperture; d) multi hole frame mounted on the aperture.

The outer reverberation chamber was fed by a log-periodic antenna (#1) and the resulting energy exciting the sample was monitored by a second antenna (#2) of the same type (Fig. 5a). The field inside the nested chamber was picked up by two double ridge antennas, receiving (#3) and transmitting (#4). A four port Vector Network Analyzer (VNA) was connected to the system to measure the scattering parameters between the four antennas: (#1) and (#2) for the outer chamber and (#3) and (#4) for the inner one. The power received was given by $|S_{ij}|^2$, where S is the complex scattering coefficient measured by the VNA, i and j are the receiving and transmitting antennas, respectively. In this case, the power received inside the outer and inside the inner reverberation chamber and the power between the outer to inner chamber were $|S_{21}|^2$, $|S_{43}|^2$ and $|S_{31}|^2$, respectively. In fact, the material exhibited also effective absorption of electromagnetic energy, thus reducing the quality factor of both reverberation chambers [62]. The SE was evaluated by:

$$SE = -10 \log \left(\frac{<|S_{21}|^2_{ns}><|S_{41}|^2_{s}><|S_{43}|^2_{ns}>}{<|S_{21}|^2_{s}><|S_{41}|^2_{ns}><|S_{43}|^2_{s}>} \right) \tag{2}$$

where $< \cdot >$ is the ensemble averaged over the chamber realizations, the subscripts *s* means “the case with the specimen” and *ns* means “the case without the specimen”. A single chamber realization of the outer RC corresponded at each stirrer position. On the contrary, within the inner chamber, due to the limited space, there was not a stirrer. In the inner chamber, a bandwidth with a frequency step of 250 kHz was considered, and the frequency stirring [63] was applied by using 400 frequency points, each of them correspondent to a chamber realisation. The investigated band was from 0.8 to 8.4 GHz, divided in several sub-bands of 400 MHz, where 1601 frequency points were acquired by the VNA, sampled by steps of 250 kHz. The stirrers worked in synchronous way; they had the same angle step and 9 stirrer positions were considered for both, 40 degrees shifted for each position.

3. Results and discussions

3.1. Mechanical and microstructural characterisation

The results of the tensile (f_{ct}) and compressive strength (R_c) of the pastes during the first 28 days of curing are reported in Table 6.

As for regards the f_{ct} values, all the pastes show the same behaviour, with a gradual increase of tensile strength during time; only FS 0.25 and FS 0.50 specimens reach approximately the maximum strength after 7 days of curing. This effect is related to the presence of alkaline salts in the foundry sand [64] (Table 1), which have operated as quick setting agents, contributing to a faster development of mechanical strength during the first days after casting.

The maximal enhancement of f_{ct} is registered for the pastes manufactured with the two commercial fillers since their strengths are 20% higher than REF if prepared with AC and more than 40% if prepared with GNP at 1.00 wt.%. Gong et al. [65] found that the use of graphene oxide (GO) inside Portland cement pastes increases the tensile strength more than the 40% when used at 0.03 wt.% on the binder content. The great strength enhancement provided by the little amount of GO used by Gong et al. is related to the great capacity of this material to be dispersed in water, being hydrophilic, compared to graphene nanoplatelets, which conversely is hydrophobic. Instead, the addition of waste carbon-based fillers (CH and FS) does not produce any effect on the tensile strength of pastes after 28 days of curing, since the results are comparable with those of REF.

Concerning compressive strength, the presence of carbonaceous fillers contributes to increase the R_c values even after 2 days of curing, compared to the REF paste. Moreover, when CH and FS are added, the values are two and three times higher, respectively. As for tensile strength, in FS pastes this behaviour is related to the presence of alkaline salts inside this waste carbon-based filler (Table 1) which act as quick setting agents. In the case of CH paste, this is probably due to the surface area of CH particles (76 m^2/g) that contributes to the growth of hydration products, giving again an accelerating effect on the hydration kinetics at early ages, as reported by Gupta and Kua [66] for cement-based mixtures. This behaviour was also detected in [67] where carbon-based fillers were added in hydraulic lime-based mortars. Furthermore, each addition at each percentage increases the final mechanical strength (R_c at 28 days) compared to the REF paste, except for AC 1.00 one, up to 45%. This high content of AC decreases the workability of the paste much more than the other fillers, due to its very high specific surface area (1800 m^2/g), so that additional water was necessary to reach a slump flow value comparable to that of the other pastes (Table 3). The additional water has changed the w/b ratio from 0.32 to 0.33 (Table 3), leading to a decrease in R_c after 28 days [68]. The ability of nano/micro fillers to increase the mechanical strength of cement-based materials already at early ages is known as "filler effect" [69]. Such materials, due to their high specific surface area [4,70], work as nucleation sites for C-S-H [71,72], accelerating the degree of hydration and therefore increasing the mechanical properties of hardened compounds. Moreover, it is well-known that the addition of fillers contributes to the refinement of the paste, lowering the total porosity (V_p) of the compound and shifting the critical pore radius (r_c) to smaller dimensions. Such effect is well visible in Table 6, where the REF paste shows a V_p of 41% whereas all other pastes have a lower total porosity value, which reaches the lowest value (36%) when FS is added. This effect is probably due to the best dispersion obtained by FS filler because of the small and spherical shape of its particles (Fig. 1d). Moreover, all the manufactured pastes are characterised by r_c smaller than the REF one, confirming the ability of all carbon-based fillers to refine the porosity of the matrix.

Table 6. Tensile strength (f_{ct}), compressive strength (R_c), total porosity (V_p) and critical pore radius (r_c) of pastes.

Mixtures	f_{ct} (MPa)			R_c (MPa)			V_p (%)	r_c (μm)
	2 days	7 days	28 days	2 days	7 days	28 days		
REF	0.20 ± 0.01	0.56 ± 0.00	0.82 ± 0.01	1.2 ± 0.0	4.2 ± 0.1	10.8 ± 0.3	41	0.116
GNP 0.25	0.30 ± 0.03	0.50 ± 0.04	0.92 ± 0.01	1.9 ± 0.0	4.8 ± 0.1	13.0 ± 0.5	37	0.082
GNP 0.50	0.30 ± 0.01	0.65 ± 0.00	0.88 ± 0.01	2.0 ± 0.1	3.5 ± 0.2	13.8 ± 0.1	39	0.103
GNP 1.00	0.40 ± 0.01	0.66 ± 0.01	1.17 ± 0.05	2.3 ± 0.2	3.7 ± 0.0	13.5 ± 0.1	39	0.104
AC 0.25	0.30 ± 0.03	0.48 ± 0.01	0.99 ± 0.00	1.2 ± 0.3	4.4 ± 0.0	12.8 ± 0.0	38	0.093

AC 0.50	0.30 ± 0.03	0.60 ± 0.01	0.97 ± 0.01	1.8 ± 0.0	4.3 ± 0.1	13.3 ± 0.1	38	0.096
AC 1.00	0.40 ± 0.01	0.58 ± 0.00	0.99 ± 0.01	1.7 ± 0.1	4.4 ± 0.1	11.1 ± 0.1	39	0.096
CH 0.25	0.34 ± 0.01	0.56 ± 0.03	0.69 ± 0.01	2.6 ± 0.1	4.2 ± 0.0	12.7 ± 0.2	38	0.111
CH 0.50	0.39 ± 0.00	0.47 ± 0.01	0.82 ± 0.02	2.7 ± 0.1	4.3 ± 0.3	12.1 ± 0.1	40	0.111
CH 1.00	0.39 ± 0.01	0.59 ± 0.03	0.82 ± 0.01	2.8 ± 0.0	5.1 ± 0.4	13.6 ± 0.1	39	0.110
FS 0.25	0.51 ± 0.01	0.85 ± 0.03	0.88 ± 0.03	3.7 ± 0.1	6.4 ± 0.2	15.8 ± 0.3	37	0.086
FS 0.50	0.57 ± 0.01	0.97 ± 0.04	0.82 ± 0.03	3.5 ± 0.2	7.5 ± 0.4	13.3 ± 0.0	36	0.084
FS 1.00	0.43 ± 0.00	0.58 ± 0.01	0.79 ± 0.01	3.0 ± 0.1	5.2 ± 0.1	13.1 ± 0.1	36	0.099

The SEM images of the REF paste and those manufactured with carbon-based fillers at 0.50 wt.% are given in Fig. 7. In AC 0.50 and FS 0.50 specimens (Figs. 7c and 7e), the presence of the carbonaceous addition is not visible, whereas in GNP 0.50 two agglomerates of graphene nanoplatelets partially embedded in the matrix can be noticed in the upper left side (Fig. 7b), confirming the higher difficulties in dispersing the GNP with respect to the other fillers. In CH 0.50 specimen, the presence of one particle of char perfectly adhered to the paste is visible in the middle area of Fig. 7d. The surface of CH particle is covered by the precipitation of hydration products, confirming again the capacity of CH to increase their growth [66].

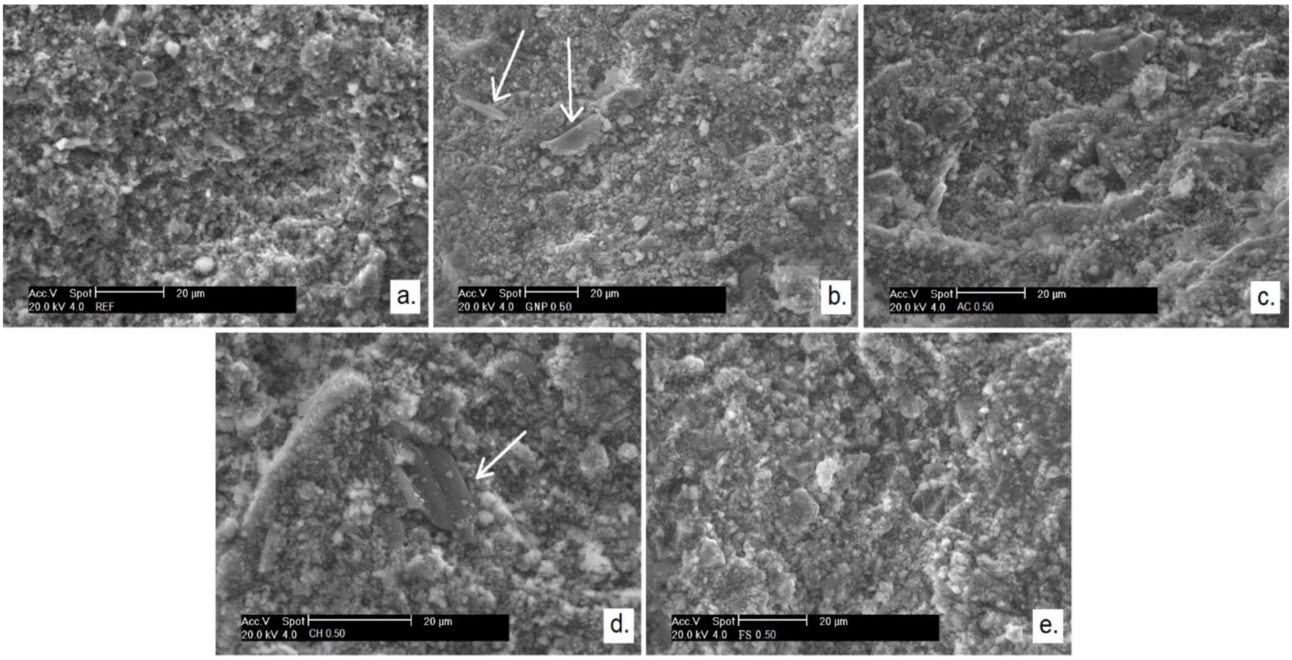

Fig. 7. SEM of pastes: a. REF; b. GNP 0.50; c. AC 050; d. CH 0.50; e. FS 0.50. Arrows indicate the carbonaceous particles.

3.2. Capillary water absorption

As for regards the water absorption coefficient (*C*) (Fig. 8), carbonaceous fillers have a great influence in decreasing the water uptake of pastes at short periods of contact with water (90 min). When GNP and FS fillers are used, *C* coefficient reaches values lower than half of that of REF. In general, increasing carbon-based fillers content, the water suction decreases, especially for pastes prepared with the two commercial fillers, since both AC [73,74] and GNP [75–77] are hydrophobic materials. This behaviour is less evident for pastes which contain CH, since their *C* values remain always around 76% of REF: this effect is related to their critical pore radii which are bigger than those of the pastes manufactured with other fillers (Table 6). The results confirm that the saturation of the capillary pores with higher dimensions occurs faster than for the smaller ones [78].

On the other hand, *C* value has a reversal trend when FS is used, seeing that it increases with the amount of this filler, with absorption values equal to 43% and 54% of REF when 0.25% and 1.00% of FS are added, respectively. The increased content of FS increases also the presence of clay impurities [64,79]; it is well-known that clay is hydrophilic and thus it is much prone to water absorption [68]. However, FS specimens show very low *C* coefficients thanks to their low total porosities and small critical pore radii r_c (Table 6).

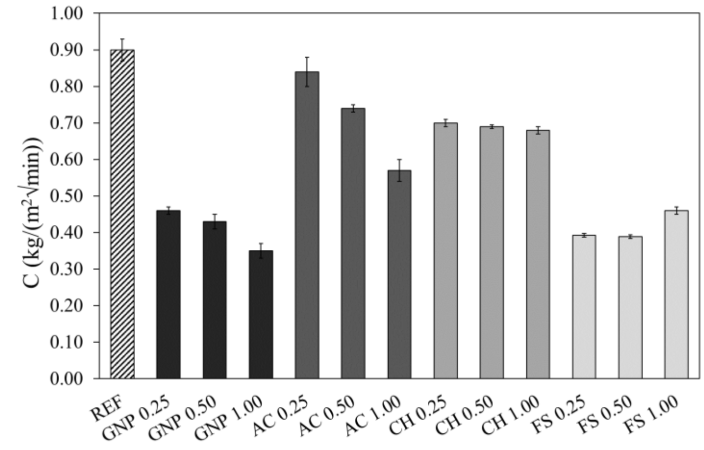

Fig. 8. Water absorption coefficient (*C*) of pastes after 28 days of curing.

The water absorbed per unit area (Q_i) by pastes after 28 days of curing is reported in Fig. 9. Also for a long time of contact with water (8 days), all specimens containing carbon-based fillers show a lower absorption compared to REF. In particular, the lowest absorptions are registered for GNP pastes (Fig. 9a), confirming again the hydrophobic nature of GNP; GNP filler, acting as a barrier against the rise of capillary water, increases the winding of the water path [48]. Also the pastes containing FS exhibit very low water absorptions in time (Fig. 9d) thanks to their lowest total porosity (Table 6). In these cases, the lowest absorptions are obtained by the specimens manufactured with 0.50 wt.% of filler. For FS 0.50 paste this is due to the smallest dimensions of the critical pore radius (Table 6); for the GNP 0.50 paste this is due to the hydrophobicity of graphene particles, since neither the total porosity nor the critical pore radius of GNP pastes are the smallest (Table 6).

The Q_i values of the pastes manufactured with AC (Fig. 9b) show an opposite trend compared to the *C* coefficient (Fig. 8). In fact, whereas the *C* coefficient increases with the AC content, the absorption decreases. This effect is related to the AC behaviour: AC is hydrophobic only at early ages thanks to its non-polar surface characteristics [80], whereas it becomes hydrophilic for long contact time with water [73].

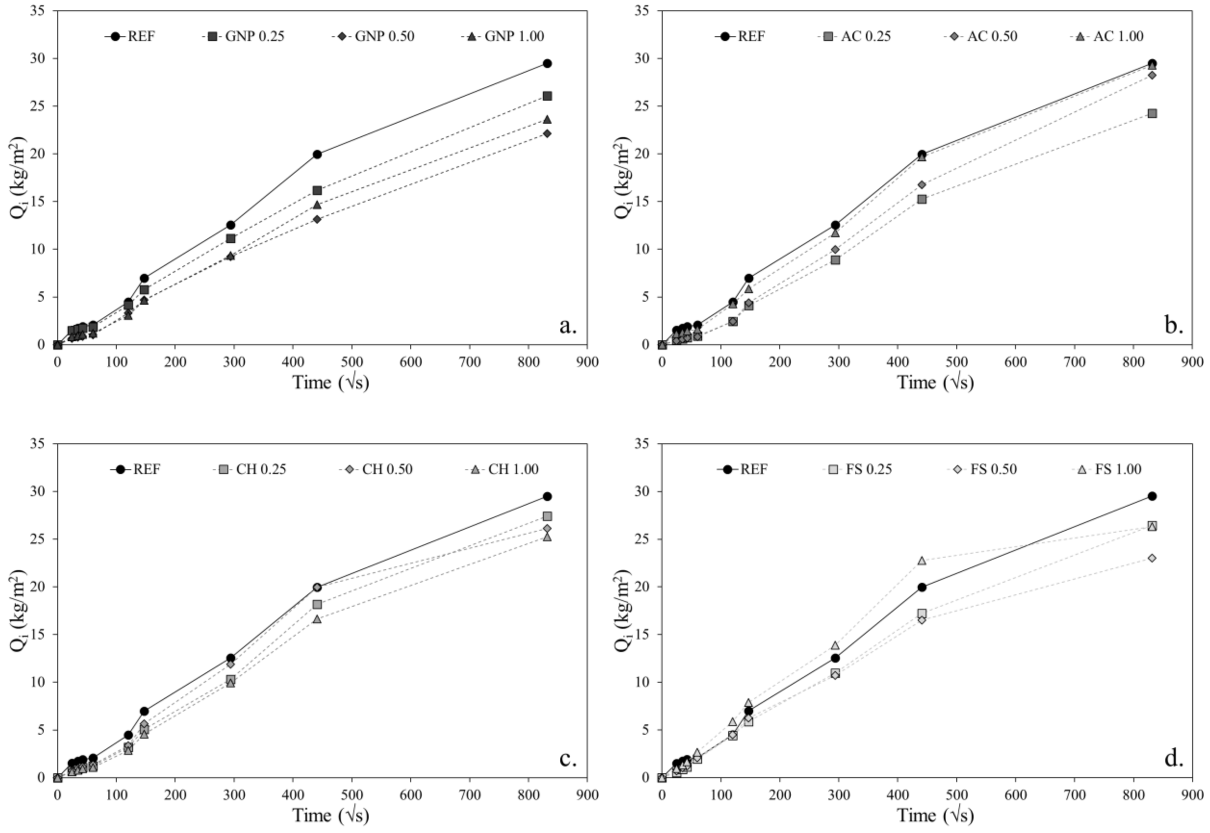

Fig. 9. Water absorbed per unit area (Q_i) of pastes after 28 days of curing. In each figure, the continuous line represents the REF paste.

3.3. Depolluting tests

3.3.1. In batch test

The depolluting capacity of the pastes under dark condition is displayed in Fig. 10, where the residual percentage of MEK inside the box is plotted against time. The trendline starts at 20 minutes because this is the time necessary for vaporising MEK completely.

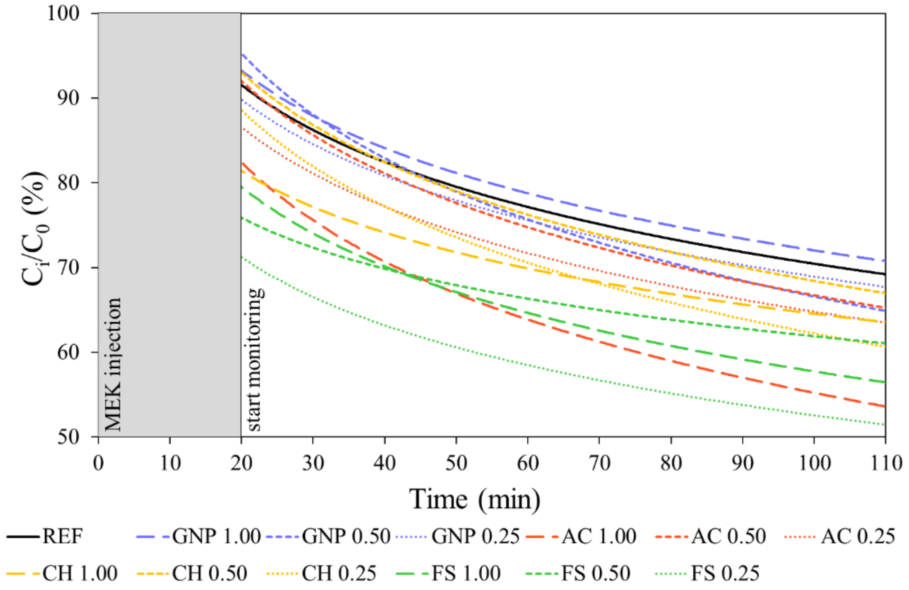

Fig. 10. Residual percentage of MEK inside the box during the in batch test carried out on pastes.

To better analyse and compare the results, in Fig. 11 the residual percentage concentration of MEK (C_i/C_0) inside the box after 110 min of test under dark condition is also reported.

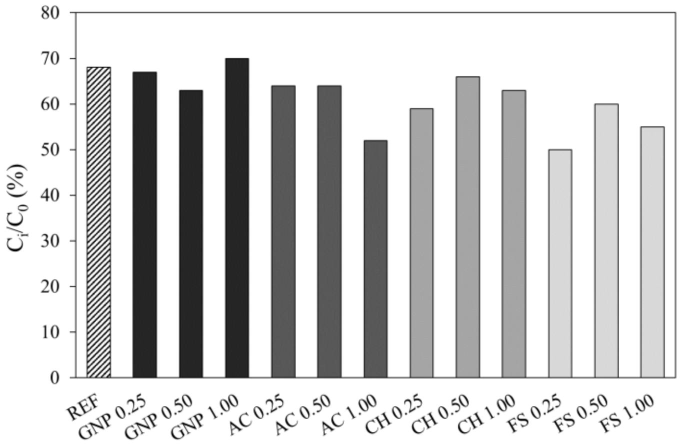

Fig. 11. Residual percentage of MEK inside the box during the in batch test on pastes after 110 min.

Fig. 10 and Fig. 11 show that under dark condition the REF paste adsorbs approximately 30% of MEK at the end of test. Only pastes manufactured with some carbonaceous fillers improve this depolluting capacity. In particular, when GNP is added the depolluting efficiency remains around 30%. AC, instead, when added at 1.00 wt.% of lime, increases the efficiency to 50%. Thanks to the great ability of AC to reduce air pollutants by adsorption [81] because of its high specific surface area (1800 m^2/g), a minimum amount of 1.00 wt.%, as in this case, is enough to obtain a significant effect. Referring to carbon waste fillers, the CH pastes show a poor effect on MEK removal, this can be ascribed to its surface area which is not so high (76 m^2/g). Even if CH is considered a potential substitute of AC for VOCs removal [34], in this case it seems not compatible for adsorbing MEK. FS appears the most effective filler to increase the depolluting capacity of pastes given that, by varying its content, residual concentrations of MEK around 40 – 50% can be achieved, even if its specific surface area (341 m^2/g) is lower than AC.

3.3.2. Flow test

The photocatalytic efficiency of the pastes tested in terms of NO_x abatement under UVA radiation is shown in Fig. 12.

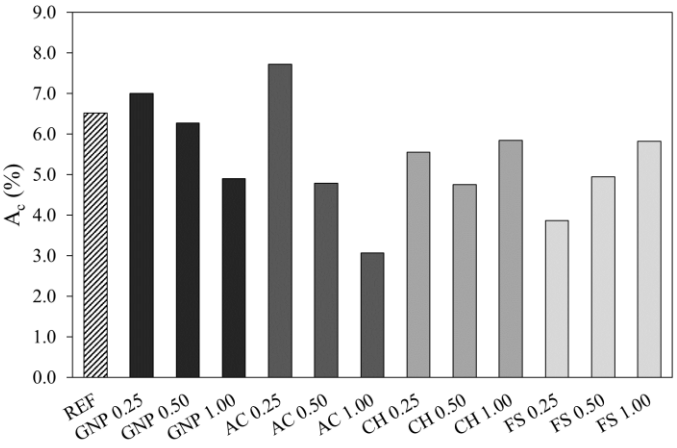

Fig. 12. Photocatalytic efficiency under UVA radiation of pastes (NO_x abatement).

Both commercial and waste carbonaceous fillers do not modify the NO_x abatement of the REF paste which is too low (6.5%) to be considered as a photocatalytic behaviour.

For the above-mentioned reason, it was decided to test some selected pastes with the addition of nano-TiO_2, that is known to be an efficient photocatalytic agent [6], in order to evaluate if the carbon-based fillers could affect the photocatalytic activity of TiO_2 improving the first stage of photoactivity (adsorption of pollutants). In fact, carbonaceous fillers could interact with the photocatalyst; keeping the surface chemistry unchanged, the increase of the specific surface area can create a high number of active sites and e^--h^+ pairs and high concentration of pollutants on the photocatalyst can be expected [82]. For this reason, some pastes were manufactured using carbonaceous fillers at 0.50 wt.% and TiO_2 at 1.00 wt.% on hydraulic lime (Table 4).

Results of the photocatalytic efficiency of the pastes with TiO_2 addition are reported in Fig. 13. When TiO_2 is added to the paste (REF T), the NO_x abatement reaches values of 25%, four times higher than that of the same paste without TiO_2 (REF specimen, Fig. 12). This result was also reported by some of the present authors in a recent paper [83], where the replacement of hydraulic lime with TiO_2 at 5 wt.% in a plain mortar contributes to enhance the photocatalytic efficiency from 5% to 35%. In general, also using carbonaceous fillers, all the pastes with TiO_2 show a great enhancement of the photocatalytic action. In particular, GNP 0.50 T and AC 0.50 T show an A_c value around 20%, which are four and three times higher than that of GNP 0.50 and AC 0.50, respectively (Fig. 12). As for regards the waste carbon-based additions, the lowest NO_x abatement is found for CH 0.50 T with an A_c value of 15%, which is three times higher than that registered for CH 0.50 specimen (Fig. 12). On the contrary, the specimen manufactured with TiO_2 and foundry sand (FS 0.50 T) shows the same photocatalytic efficiency of REF T, five times higher than that of the same paste without photocatalytic agent (Fig. 12).

Observing the results of Fig. 12 and Fig. 13, it is evident that the addition of a photocatalytic agent is necessary to obtain the photocatalytic abatement of NO_x under UVA irradiation. The results demonstrate that the addition of carbonaceous fillers, without specific treatments, is not able to increase the photocatalytic behaviour of TiO_2. For example, with GNP this effect can be only achieved by using a functionalisation method [84], like hydrothermal [85] or sol-gel [86] treatments. Moreover, the addition of carbonaceous fillers always worsens the depollution behaviour of pastes compared to the reference one: only in the case of FS, the paste shows a result comparable to the reference one, whereas the photocatalytic efficiency decreases by 20% in the case of GNP and AC addition, and even 40% in the case of CH addition. This effect could be related to the colouration that the specimens acquire because of the presence of the fillers, since their black colour has darkened the paste (Fig. 14). Only the one manufactured with FS shows a colour similar to that of REF T (Fig. 14a and 14c). It is reported that the addition of pigments, that provide a significant coloration on finishing products, can induce a moderate decrease of the photocatalytic activity in terms of NO_x abatement [87,88]. This result was also reported in [83], where the use of activated carbon in place of natural sand in TiO_2-rich hydraulic lime based mortars resulted in a decrease of the photocatalytic efficiency of about 40%, because the reduced reflectance of radiation of the darkened substrate has lowered the photocatalytic properties of the mortar [89].

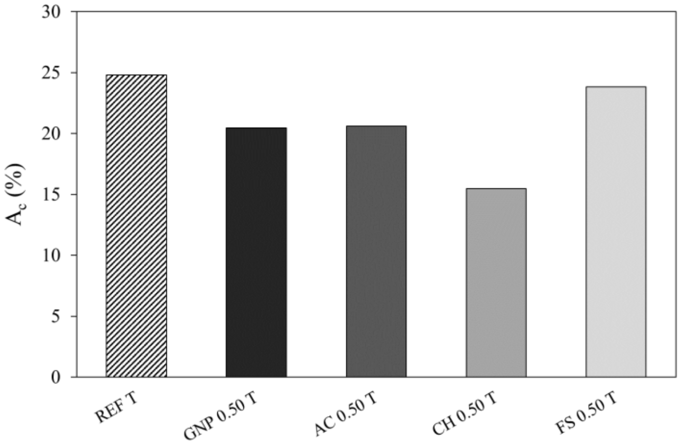

Fig. 13. Photocatalytic efficiency under UVA radiation of pastes (NO_x abatement) with TiO_2 addition.

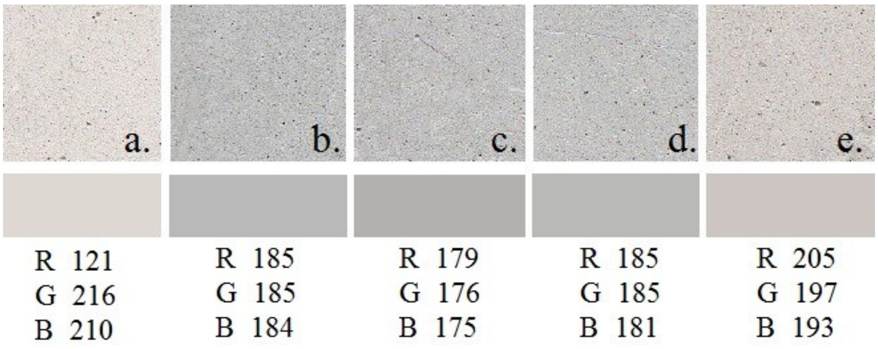

Fig. 14. Scan images of the specimens' surface (up) and average RGB value measured in five different points (down): a. REF T, b. GNP 0.50 T, c. AC 0.50 T, d. CH 0.50 T, e. FS 0.50 T.

3.4. Electromagnetic characterization

3.4.1. Electrical resistivity

The DC electrical resistivity (ρ) measurements conducted on the paste specimens at 7, 14, 21 and 28 days of curing are displayed in Fig. 15.

After the first week (Fig. 15a), the REF paste registers an electrical resistivity of 170 Ω·cm. All the other pastes show similar ρ values ranging from 190 to 170 Ω·cm, unless that prepared with the FS filler, which shows a higher electrical resistivity. Moving towards 0.25 to 0.50 and 1.00 percentages of FS, the electrical resistivity decreases with values equal to 790, 360 and 210 Ω·cm, respectively. However, in these pastes the electrical resistivity decreases by increasing FS addition, as reported in literature for GNP [2], carbon black [49,54], carbon coke [53] and graphite [14] additions.

After 14 days, the electrical resistivity of pastes increases of one order of magnitude (Fig. 15b). The ρ measured in the REF paste is about 3400 Ω·cm, whereas all the other specimens with carbon-based additions show a lower electrical resistivity. In general, a clear trend related to the different additions of the same filler and electrical resistivity is not visible; in fact, only those with FS maintain the trend observed at 7 days of curing.

After 21 days from casting (Fig. 15c), ρ values continue to increase, especially for REF paste, achieving approximately 10000 Ω·cm. Also at this curing period, all pastes containing carbonaceous fillers assume lower values of ρ than REF, even if those manufactured with GNP show an opposite trend compared to that reported in literature since the higher the amount of the carbon-based fillers, the higher the resistivity. This effect could be related to the agglomeration of GNP particles [28,90,91], as observed in Fig. 7. It is reported that the decrease of electrical resistivity with the increase of carbon-based fillers dosage is obtained only when the amount remains under the percolation threshold and the particles are well dispersed or, above this value, a further decrease of electrical resistivity occurs only if fillers segregate along the continuous conduction paths [92]. The percolation threshold is the volume fraction above which the adjacent admixture units, whether fibres or particles, touch the one to another forming a continuous conduction path [54]. For GNP, the percolation threshold has been found to be between 10 and 15 wt.% by cement [2], much higher than the amount of GNP used in the present paper. When AC is used, ρ shows a decrease from 0.25 to 0.50 wt.% AC addition and then ρ increases at 1.00 wt.% addition. It is possible that also for the AC paste, the increase of ρ values is due to the agglomeration of particles which have discontinued the available current paths. As for regards the waste carbon fillers, the electrical resistivity of CH specimens, regardless the addition amount, is approximately 4000 Ω·cm which is 60% lower than REF, whereas FS specimens continue to maintain the same trend registered at previous ages.

After 28 days (Fig. 15d) the electrical resistivity increases again and, for REF paste it doubles the value registered at 21 days reaching 22000 Ω·cm. For the specimens with carbonaceous additions, the trend measured at 21 days is confirmed. In general, at 21 and 28 days of curing, the lowest ρ values (approximately 65% lower than REF) are found for GNP 0.25, for all specimens manufactured with CH, and for FS 1.00 paste.

The good electrical properties given by carbon-based addition are related to both their carbon content, which is high especially for GNP and AC, and to their good dispersion within the matrix, as in the case of waste CH and FS fillers.

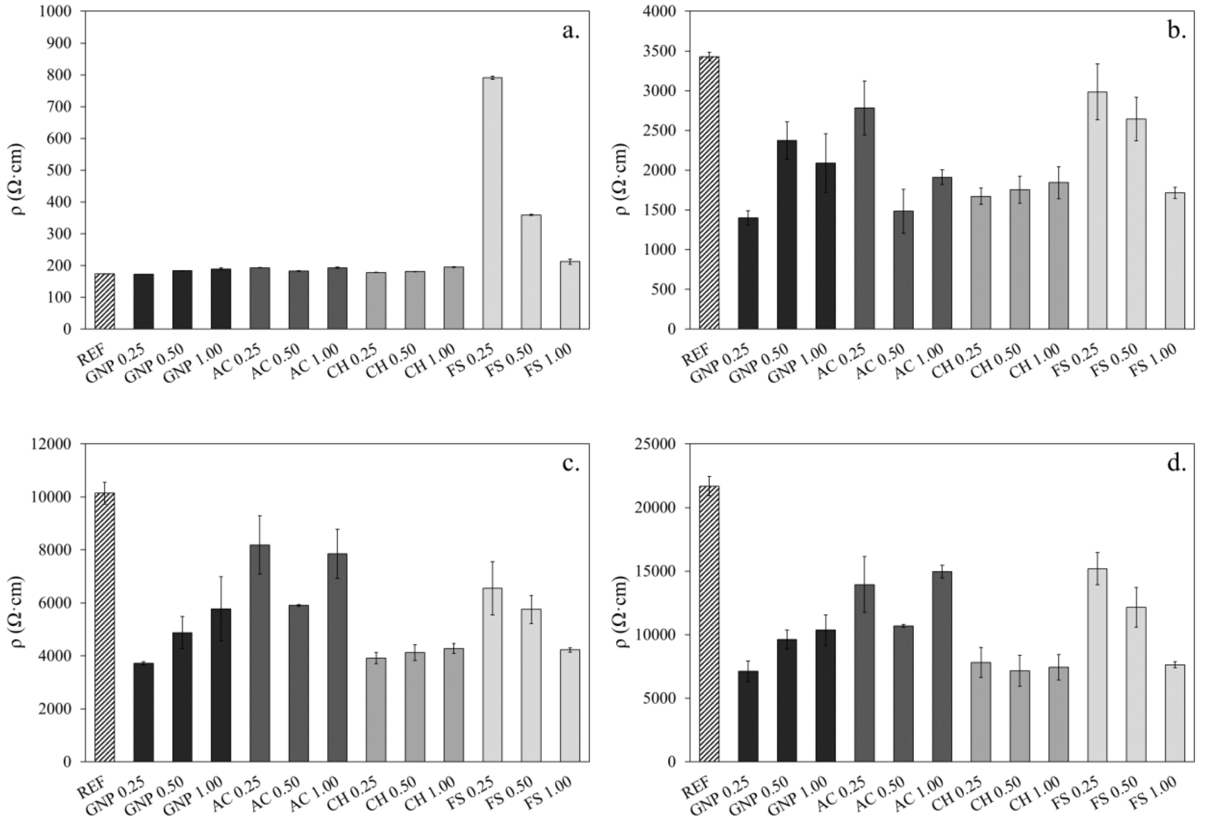

Fig. 15. DC electrical resistivity (ρ) of pastes after: a. 7, b. 14, c. 21, d. 28 days of curing.

3.4.1. Electromagnetic shielding property

Generally, the electromagnetic shielding property increases with electrical conductivity. Since the lowest electrical resistivity values were found in pastes with waste carbonaceous fillers at the highest percentages (1.00 wt.%) and commercial fillers at 0.50 wt.%, the SE was determined only for these mixes. However, SE was measured not on pastes but on mortars (Table 5) since a perfect adhesion between the specimens and the mould used for the test shall be ensured and mortars shrink less than pastes.

The obtained results are given in Fig. 16. It should be stressed that in literature, there is no paper considering the behaviour of carbonaceous additions on the SE of lime-based mortars. In general, the SE of the present mortars is similar to that of cement-based mixes [33], as shown also by Samková et al. [93] who tested plasters manufactured with different binders and found that the SE of plain cement- and lime-based pastes was comparable. All mortars with carbonaceous additions register a higher, or at least similar, SE compared to that of M REF; in particular, M GNP 0.50 mortar always shows a SE 1 or 2 dB higher than the reference one. Only M AC 0.50 mortar shows a lower SE than M REF at each investigated frequency value.

In order to analyse the obtained results in detail, Fig. 17 shows figures enlarged at 2 – 3 GHz, 4 – 5 GHz and 6 – 7 GHz, since in these frequency ranges the differences between mortars are more visible. These frequencies are mostly familiar with wireless communication systems. Frequencies of 2.1 GHz and 2.6 GHz are used for telecommunication mobile phones, Universal Mobile Telecommunications System (UMTS) and fourth generation Long Term Evolution (4G-LTE), respectively. Moreover, 2.45 GHz for the Bluetooth standard, whereas 2.4 GHz and 5 GHz are used for wireless networks. The frequency of 7 GHz is dedicated for point-to-point narrow band systems, as Plesiochronous Digital Hierarchy/Synchronous Digital Hierarchy (PDH/SDH). In these frequency ranges, M GNP 0.50 increases SE of about 30% compared to M REF. Also the carbon-based waste fillers enhance the SE at 2 – 3 GHz, 4 – 5 GHz and 6 – 7 GHz compared to the M REF mortar, even though the best improvement is around 6% for M CH 1.00 mortar. These results confirm that the fillers giving the lowest electrical resistivity to the pastes are also those giving the highest SE values. In general, the high specific surface area, the high chemical stability and the high conductivity of graphene have been reported to be the key parameters for its good EM wave absorption properties [94,95]. It has been found that a low dosage of GNP equal to 0.1 wt.% is able to increase the electromagnetic wave absorption of cement-based materials [94]. Therefore, even if GNP is surely the most effective filler for enhancing the electromagnetic shielding properties of binder-based materials, in this study also priceless waste carbonaceous fillers can improve this property [33]. The increased electromagnetic SE of the mortar containing CH filler is due to its very good dispersion, which has formed a connected and conductive network able to enhance the electrical conductivity of the material and to the enhanced interfacial polarization of CH, as found by Mahmood et al. [96] who obtained the best SE by using carbonized cotton stalk in mortars at 0.5 wt.% by cement.

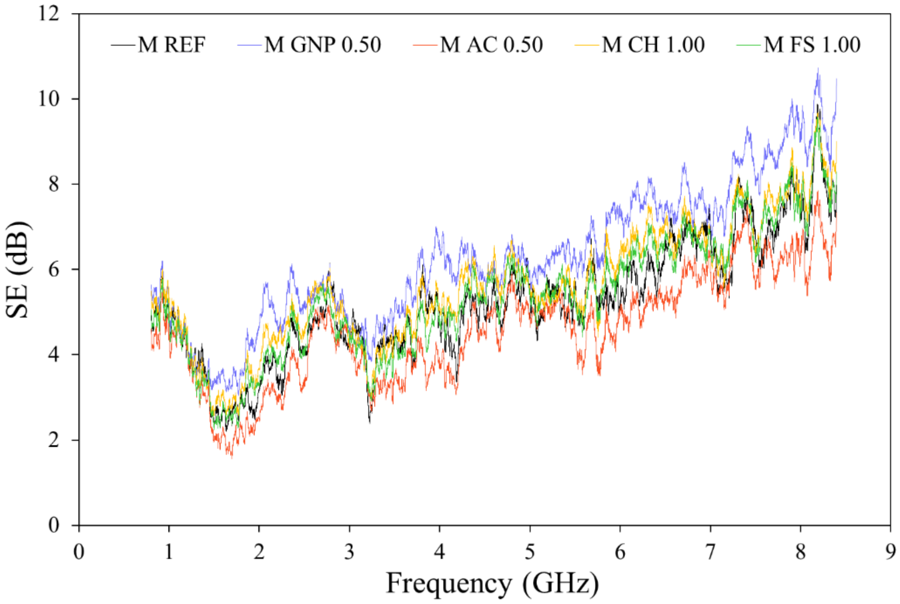

Fig. 16. Shielding effectiveness (SE) of mortars after 21 days of curing.

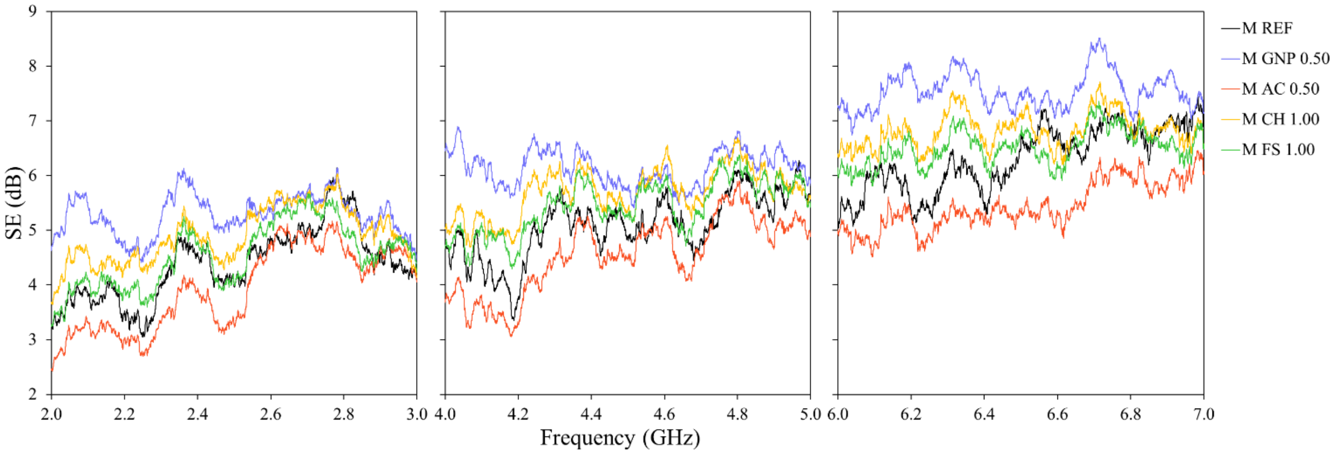

Fig. 17. Shielding effectiveness (SE) of mortars after 21 days of curing in the ranges of frequencies between 2 – 3, 4 – 5 and 6 – 7 GHz.

4. Conclusions

The use of commercial and waste carbon-based micro-fillers was investigated in order to improve the mechanical, durability, depolluting, electrical and electromagnetic properties of hydraulic lime-based pastes and mortars. As commercial fillers, graphene nanoplatelets (GNP) and powdered activated carbon (AC) were used. As priceless wastes, a char (CH) obtained by the gasification process of biomasses and the finest fraction of a used foundry sand (FS) were chosen. Fillers were added at 0.25, 0.50 and 1.00 % on lime weight.

The obtained results suggest the following conclusions:

- The addition of carbonaceous fillers, regardless of their nature and amount, is essential to reduce the total porosity and the critical pore radius of pastes. The resulting "filler effect" enhances the tensile strength of 40% and 20% when GNP and AC are added at 1.00 wt.% on the lime, respectively. Particularly the compressive strength is increased for all the type of additions, both commercial and waste up to 45%.
- The reduced porosity and the smaller critical pore radius lower the capillary water absorption of pastes at each percentage and type of carbonaceous addition, both at short and long time of contact with water. At early ages, the capillary water absorption is decreased more than 50% with GNP and FS.
- The depollution capacity of the pastes, in terms of MEK adsorption, enhances mostly by the addition of AC at 1.00 wt.%. However, both the waste fillers, at all percentages, show very good adsorption capacity, even equal to 50% when FS is added.
- No one of the carbonaceous fillers is effective to produce a photocatalytic activity to the pastes when a photocatalytic agent is absent. Under UVA radiation and in the presence of TiO_2, the carbonaceous fillers even decrease the photocatalytic behaviour because of the darkening of the paste.
- Both the commercial and waste carbon-based fillers decrease the electrical resistivity of the lime pastes; in particular, the use of CH decreases the electrical resistivity up to 65% as for GNP at 0.25 wt.% and FS at 1.00 wt.%. This finding could be interesting for the development of the so called "self-sensing" mortars/concretes.
- The highest EMI SE have been found for mortars containing GNP and CH; in particular, the SE is enhanced by 6% in case of CH and even by 30% in case of GNP.

For the above-described results, it can be affirmed that addition of cheap waste carbon-based fillers, such as gasification char and the finest fraction of a used foundry sand, can be a better alternative in terms of cost/efficiency to more expensive and less sustainable commercial carbon based fillers, as graphene nanoplatelets and activated carbon, to improve several properties of lime-based pastes/mortars. In fact, the price of GNP is approximately 370 €/kg and the price of AC is around 260 €/kg, whereas CH and FS, being wastes, have no commercial value. In particular, in the present work it has been found that waste carbonaceous fillers are able to increase the mechanical strength, the durability in terms of capillary water absorption, the depolluting capacity in terms of VOCs adsorption, the electrical conductivity and, even if slightly, the shielding effectiveness of lime-based pastes/mortars that can be used for indoor renders and panels.

Acknowledgements

The authors wish to thank Pentachem S.r.l. for the graphene nanoplatelets, Cabot Norit Nederland B.V. for the activated carbon, LA.BO S.r.l. for the used foundry sand kindly offered for this work, and DIASEN S.r.l. to have co-financed a Ph.D. fellowship on "Carbon based fillers for the development of innovative multifunctional mortars and plasters" (Eng. Alberto Belli).

References

[1] A. Mohammed, J.G. Sanjayan, W.H. Duan, A. Nazari, Incorporating graphene oxide in cement composites: A study of transport properties, Constr. Build. Mater. 84 (2015) 341–347. doi:10.1016/j.conbuildmat.2015.01.083.

[2] J.-L. Le, H. Du, S.D. Pang, Use of 2D Graphene Nanoplatelets (GNP) in cement composites for structural health evaluation, Compos. Part B Eng. 67 (2014) 555–563. doi:10.1016/j.compositesb.2014.08.005.

[3] D.D.L. Chung, Carbon materials for structural self-sensing, electromagnetic shielding and thermal interfacing, Carbon N. Y. 50 (2012) 3342–3353. doi:10.1016/j.carbon.2012.01.031.

[4] S. Chuah, Z. Pan, J.G. Sanjayan, C.M. Wang, W.H. Duan, Nano reinforced cement and concrete composites and new perspective from graphene oxide, Constr. Build. Mater. 73 (2014) 113–124. doi:10.1016/j.conbuildmat.2014.09.040.

[5] B. Han, S. Sun, S. Ding, L. Zhang, X. Yu, J. Ou, Review of nanocarbon-engineered multifunctional cementitious composites, Compos. Part A Appl. Sci. Manuf. 70 (2015) 69–81. doi:10.1016/j.compositesa.2014.12.002.

[6] F. Pacheco-Torgal, S. Jalali, Nanotechnology: Advantages and drawbacks in the field of construction and building materials, Constr. Build. Mater. 25 (2011) 582–590. doi:10.1016/j.conbuildmat.2010.07.009.

[7] D. Micheli, R. Pastore, A. Vricella, R.B. Morles, M. Marchetti, A. Delfini, F. Moglie, V. Mariani Primiani, Electromagnetic characterization and shielding effectiveness of concrete composite reinforced with carbon nanotubes in the mobile phones frequency band, Mater. Sci. Eng. B. 188 (2014) 119–129. doi:10.1016/j.mseb.2014.07.001.

[8] C. Giosuè, M. Pierpaoli, A. Mobili, M.L. Ruello, F. Tittarelli, Influence of Binders and Lightweight Aggregates on the Properties of Cementitious Mortars: From Traditional Requirements to Indoor Air Quality Improvement, Materials (Basel). 10 (2017) 978. doi:10.3390/ma10080978.

[9] S.E. Frey, H. Destaillats, S. Cohn, S. Ahrentzen, M.P. Fraser, The effects of an energy efficiency retrofit on indoor air quality, Indoor Air. 25 (2015) 210–219. doi:10.1111/ina.12134.

[10] C. Beall, E. Delzell, P. Cole, I. Brill, Brain Tumors among Electronics Industry Workers, Epidemiology. 7 (1996) 125–130. http://journals.lww.com/epidem/abstract/1996/03000/brain_tumors_among_electronics_industry_workers.4.aspx.

[11] K.W. Andrews, D.A. Savitz, Accuracy of industry and occupation on death certificates of electric utility workers: Implications for epidemiologic studies of magnetic fields and cancer,

Bioelectromagnetics. 20 (1999) 512–518. doi:10.1002/(SICI)1521-186X(199912)20:8<512::AID-BEM5>3.0.CO;2-M.

[12] H. Guan, S. Liu, Y. Duan, J. Cheng, Cement based electromagnetic shielding and absorbing building materials, Cem. Concr. Compos. 28 (2006) 468–474. doi:10.1016/j.cemconcomp.2005.12.004.

[13] J. Chen, D. Zhao, H. Ge, J. Wang, Graphene oxide-deposited carbon fiber/cement composites for electromagnetic interference shielding application, Constr. Build. Mater. 84 (2015) 66–72. doi:10.1016/j.conbuildmat.2015.03.050.

[14] J. Cao, D.D.L. Chung, Colloidal graphite as an admixture in cement and as a coating on cement for electromagnetic interference shielding, Cem. Concr. Res. 33 (2003) 1737–1740. doi:10.1016/S0008-8846(03)00152-2.

[15] L. Zhong, F. Haghighat, Photocatalytic air cleaners and materials technologies - Abilities and limitations, Build. Environ. 91 (2015) 191–203. doi:10.1016/j.buildenv.2015.01.033.

[16] C. Giosuè, A. Belli, A. Mobili, B. Citterio, F. Biavasco, M.L. Ruello, F. Tittarelli, Improving the Impact of Commercial Paint on Indoor Air Quality by Using Highly Porous Fillers, Buildings. 7 (2017) 110. doi:10.3390/buildings7040110.

[17] S. Lorencik, Q.L. Yu, H.J.H. Brouwers, Photocatalytic coating for indoor air purification: Synergetic effect of photocatalyst dosage and silica modification, Chem. Eng. J. 306 (2016) 942–952. doi:10.1016/j.cej.2016.07.093.

[18] D.D.L. Chung, Electromagnetic interference shielding effectiveness of carbon materials, Carbon N. Y. 39 (2001) 279–285. doi:10.1016/S0008-6223(00)00184-6.

[19] M.-H. Lai, R.Q. Chu, H.-C. Huang, S.-H. Shu, T.-W. Chung, Equilibrium Isotherms of Volatile Alkanes, Alkenes, and Ketones on Activated Carbon, J. Chem. Eng. Data. 54 (2009) 2208–2215. doi:10.1021/je800826d.

[20] L. Li, P.A. Quinlivan, D.R.U. Knappe, Effects of activated carbon surface chemistry and pore structure on the adsorption of organic contaminants from aqueous solution, Carbon N.

Y. 40 (2002) 2085–2100.

[21] N.J. Krou, I. Batonneau-Gener, T. Belin, S. Mignard, I. Javierre, I. Dubois-Brugger, Reactivity of volatile organic compounds with hydrated cement paste containing activated carbon, Build. Environ. 87 (2015) 102–107. doi:10.1016/j.buildenv.2015.01.025.

[22] M. Horgnies, E.M. Gartner, NOx de-pollution by hardened concrete and the influence of activated charcoal additions, Cem. Concr. Res. 42 (2012) 1348–1355. doi:10.1016/j.cemconres.2012.06.007.

[23] K. Jin, J. Miyawaki, N. Shiratori, S. Yoon, J. Jang, Toward an effective adsorbent for polar pollutants: Formaldehyde adsorption by activated carbon, J. Hazard. Mater. 260 (2013) 82–88. doi:10.1016/j.jhazmat.2013.04.049.

[24] J. Wu, D.D.L. Chung, Increasing the electromagnetic interference shielding effectiveness of carbon fiber polymer – matrix composite by using activated carbon fibers, Carbon N. Y. 40 (2002) 445–447.

[25] G. Srinivas, Z.X. Guo, Graphene-based materials: Synthesis and gas sorption, storage and separation, Prog. Mater. Sci. 69 (2014) 1–60. doi:10.1016/j.pmatsci.2014.10.004.

[26] Q. Liu, Q. Xu, Q. Yu, R. Gao, T. Tong, Experimental investigation on mechanical and piezoresistive properties of cementitious materials containing graphene and graphene oxide nanoplatelets, Constr. Build. Mater. 127 (2016) 565–576. doi:10.1016/j.conbuildmat.2016.10.024.

[27] H. Du, S.D. Pang, Mechanical Response and Strain Sensing of Cement Composites Added with Graphene Nanoplatelet Under Tension, in: K. Sobolev, V. Shah (Eds.), Nanotechnol. Constr., Springer, Cham, 2015: pp. 377–382. doi:10.1007/978-3-319-17088-6.

[28] A. Belli, A. Mobili, T. Bellezze, F. Tittarelli, P.B. Cachim, Evaluating the self-sensing ability of cement mortars manufactured with graphene nanoplatelets, virgin or recycled carbon fibers through piezoresistivity tests, Sustainability. 10 (2018) 4013. doi:10.3390/su10114013.

[29] S. Wen, D.D.L. Chung, Piezoresistivity-based strain sensing in carbon fiber-reinforced

cement, ACI Mater. J. 104 (2007) 171–179.

[30] X. Zhang, B. Gao, A. Elise, C. Cao, Y. Li, Adsorption of VOCs onto engineered carbon materials: A review, J. Hazard. Mater. 338 (2017) 102–123. doi:10.1016/j.jhazmat.2017.05.013.

[31] X. Zhen, W.C. Ng, Y.W. Tong, Y. Dai, K.G. Neoh, C.-H. Wang, Toxicity assessment of carbon black waste: A by-product from oil refineries, J. Hazard. Mater. 321 (2017) 600–610. doi:10.1016/j.jhazmat.2016.09.043.

[32] V.M. Harik, Geometry of carbon nanotubes and mechanisms of phagocytosis and toxic effects, Toxicol. Lett. 273 (2017) 69–85. doi:10.1016/j.toxlet.2017.03.016.

[33] R.A. Khushnood, S. Ahmad, P. Savi, J.M. Tulliani, M. Giorcelli, G.A. Ferro, Improvement in electromagnetic interference shielding effectiveness of cement composites using carbonaceous nano/micro inerts, Constr. Build. Mater. 85 (2015) 208–216. doi:10.1016/j.conbuildmat.2015.03.069.

[34] V. Benedetti, F. Patuzzi, M. Baratieri, Gasification char as a potential substitute of activated carbon in adsorption applications, Energy Procedia. 105 (2017) 712–717. doi:10.1016/j.egypro.2017.03.380.

[35] A. Sirico, P. Bernardi, B. Belletti, A. Malcevschi, E. Dalcanale, I. Domenichelli, P. Fornoni, E. Moretti, Mechanical characterization of cement-based materials containing biochar from gasification, Constr. Build. Mater. 246 (2020) 118490. doi:10.1016/j.conbuildmat.2020.118490.

[36] D. Maskell, C.F. da Silva, K. Mower, R. Cheta, A. Dengel, R. Ball, M. Ansell, P. Walker, A. Shea, Properties of bio-based insulation materials and their potential impact on indoor air quality, in: First Int. Conf. Bio-Based Build. Mater., Clermont-Ferrand, France, 2015: pp. 1–8.

[37] C. Giosuè, A. Mobili, G. Toscano, M.L. Ruello, F. Tittarelli, Effect of Biomass Waste Materials as Unconventional Aggregates in Multifunctional Mortars for Indoor Application,

Procedia Eng. 161 (2016) 655–659. doi:10.1016/j.proeng.2016.08.724.

[38] H. Bilal, M. Yaqub, S.K.U. Rehman, M. Abid, R. Alyousef, H. Alabduljabbar, F. Aslam, Performance of Foundry Sand Concrete under Ambient and Elevated Temperatures, Materials (Basel). 12 (2019) 2645. doi:10.3390/ma12162645.

[39] R. Siddique, G. Singh, R. Belarbi, K. Ait-Mokhtar, Comparative investigation on the influence of spent foundry sand as partial replacement of fine aggregates on the properties of two grades of concrete, Constr. Build. Mater. 83 (2015) 216–222. doi:10.1016/j.conbuildmat.2015.03.011.

[40] B. Bhardwaj, P. Kumar, Waste foundry sand in concrete: A review, Constr. Build. Mater. 156 (2017) 661–674. doi:10.1016/j.conbuildmat.2017.09.010.

[41] J. Válek, E. Van Halem, A. Viani, M. Pérez-Estébanez, R. Ševčík, P. Šašek, Determination of optimal burning temperature ranges for production of natural hydraulic limes, Constr. Build. Mater. 66 (2014) 771–780. doi:10.1016/j.conbuildmat.2014.06.015.

[42] P. Faria, P. Duarte, D. Barbosa, I. Ferreira, New composite of natural hydraulic lime mortar with graphene oxide, Constr. Build. Mater. 156 (2017) 1150–1157. doi:10.1016/j.conbuildmat.2017.09.072.

[43] M.M. Barbero-Barrera, N.F. Medina, C. Guardia-Martín, Influence of the addition of waste graphite powder on the physical and microstructural performance of hydraulic lime pastes, Constr. Build. Mater. 149 (2017) 599–611. doi:10.1016/j.conbuildmat.2017.05.156.

[44] A. Mobili, C. Giosuè, T. Bellezze, G.M. Revel, F. Tittarelli, Gasification Char and Used Foundry Sand as Alternative Fillers to Graphene Nanoplatelets for Electrically Conductive Mortars with and without Virgin/Recycled Carbon Fibres, Appl. Sci. 11 (2021) 50. doi:10.3390/app11010050.

[45] T.-C. Hou, V.K. Nguyen, Y.-M. Su, Y.-R. Chen, P.-J. Chen, Effects of coarse aggregates on the electrical resistivity of Portland cement concrete, Constr. Build. Mater. 133 (2017) 397–408. doi:10.1016/j.conbuildmat.2016.12.044.

[46] A. Mazzoli, O. Favoni, Particle size, size distribution and morphological evaluation of airborne dust particles of diverse woods by Scanning Electron Microscopy and image processing program, Powder Technol. 225 (2012) 65–71. doi:10.1016/j.powtec.2012.03.033.

[47] A. Mazzoli, G. Moriconi, Particle size, size distribution and morphological evaluation of glass fiber reinforced plastic (GRP) industrial by-product, Micron. 67 (2014) 169–178. doi:10.1016/j.micron.2014.07.007.

[48] H. Du, S.D. Pang, Enhancement of barrier properties of cement mortar with graphene nanoplatelet, Cem. Concr. Res. 76 (2015) 10–19. doi:10.1016/j.cemconres.2015.05.007.

[49] Y. Dai, M. Sun, C. Liu, Z. Li, Electromagnetic wave absorbing characteristics of carbon black cement-based composites, Cem. Concr. Compos. 32 (2010) 508–513. doi:10.1016/j.cemconcomp.2010.03.009.

[50] A. Mobili, C. Giosuè, V. Corinaldesi, F. Tittarelli, Bricks and Concrete Wastes as Coarse and Fine Aggregates in Sustainable Mortars, Adv. Mater. Sci. Eng. 2018 (2018). doi:10.1155/2018/8676708.

[51] A. Mobili, C. Giosuè, F. Tittarelli, Valorisation of GRP Dust Waste in Fired Clay Bricks, Adv. Civ. Eng. 2018 (2018). doi:10.1155/2018/5256741.

[52] F. Tittarelli, C. Giosuè, A. Mobili, M.L. Ruello, Influence of binders and aggregates on VOCs adsorption and moisture buffering activity of mortars for indoor applications, Cem. Concr. Compos. 57 (2015) 75–83. doi:10.1016/j.cemconcomp.2014.11.013.

[53] J. Cao, D.D.L. Chung, Coke powder as an admixture in cement for electromagnetic interference shielding, Carbon N. Y. 41 (2003) 2433–2436. doi:10.1016/S0008-6223(03)00289-6.

[54] S. Wen, D.D.L. Chung, Partial replacement of carbon fiber by carbon black in multifunctional cement-matrix composites, Carbon N. Y. 45 (2007) 505–513. doi:10.1016/j.carbon.2006.10.024.

[55] D.D.L. Chung, Multifunctional Cement-Based Materials, CRC Press, 2003.

[56] A. Belli, A. Mobili, T. Bellezze, F. Tittarelli, Commercial and recycled carbon/steel fibers for fiber-reinforced cement mortars with high electrical conductivity, Cem. Concr. Compos. 109 (2020) 103569. doi:10.1016/j.cemconcomp.2020.103569.

[57] D.L. Lide, Handbook of Chemistry and Physics, 82nd ed., CRC Press, Boca Raton, Florida, USA, 2001.

[58] D.A. Hill, Electromagnetic Theory of Reverberation Chambers, NIST Technical Note 1506, National Institute of Standards and Technology, Boulder, Colorado, 1998. http://ws680.nist.gov/publication/get_pdf.cfm?pub_id=24427.

[59] D. Micheli, A. Vricella, R. Pastore, A. Delfini, R. Bueno Morles, M. Marchetti, F. Santoni, L. Bastianelli, F. Moglie, V. Mariani Primiani, V. Corinaldesi, A. Mazzoli, J. Donnini, Electromagnetic properties of carbon nanotube reinforced concrete composites for frequency selective shielding structures, Constr. Build. Mater. 131 (2017) 267–277. doi:10.1016/j.conbuildmat.2016.11.078.

[60] C.L. Holloway, D.A. Hill, J. Ladbury, G. Koepke, R. Garzia, Shielding effectiveness measurements of materials using nested reverberation chambers, IEEE Trans. Electromagn. Compat. 45 (2003) 350–356. doi:10.1109/TEMC.2003.809117.

[61] M. Albano, D. Micheli, G. Gradoni, R.B. Morles, M. Marchetti, F. Moglie, V. Mariani Primiani, Electromagnetic shielding of thermal protection system for hypersonic vehicles, Acta Astronaut. 87 (2013) 30–39. doi:10.1016/j.actaastro.2013.02.003.

[62] L. Bastianelli, S. Capra, G. Gradoni, D. Micheli, A. Vricella, V. Corinaldesi, A. Mazzoli, F. Moglie, V.M. Primiani, Shielding effectiveness statistical evaluation of random concrete composites, in: 3rd IEEE Int. Work. Metrol. Aerospace, Metroaerosp., IEEE, 2016: pp. 172–176. doi:10.1109/MetroAeroSpace.2016.7573207.

[63] D.A. Hill, Electronic Mode Stirring for Reverberation Chambers, IEEE Trans. Electromagn. Compat. 36 (1994) 294–299. doi:10.1109/15.328858.

[64] S. Monosi, F. Tittarelli, C. Giosuè, M.L. Ruello, Effect of two different sources and washing

treatment on the properties of UFS by-products for mortar and concrete production, Constr. Build. Mater. 44 (2013) 260–266. doi:10.1016/j.conbuildmat.2013.02.029.

[65] K. Gong, S.M. Asce, Z. Pan, A.H. Korayem, D. Ph, L. Qiu, D. Li, F. Collins, C.M. Wang, W.H. Duan, a M. Asce, Reinforcing Effects of Graphene Oxide on Portland Cement Paste, J. Mater. Civ. Eng. vol 27 (2014) 1–6. doi:10.1061/(ASCE)MT.1943-5533.0001125.

[66] S. Gupta, H.W. Kua, Carbonaceous micro-filler for cement: Effect of particle size and dosage of biochar on fresh and hardened properties of cement mortar, Sci. Total Environ. 662 (2019) 952–962. doi:10.1016/j.scitotenv.2019.01.269.

[67] C. Giosuè, A. Mobili, B. Citterio, F. Biavasco, M.L. Ruello, F. Tittarelli, Innovative hydraulic lime-based finishes with unconventional aggregates and TiO2 for the improvement of indoor air quality, Manuf. Rev. 7 (2020) 1–9. doi:10.1051/mfreview/2020010.

[68] M. Collepardi, The new concrete, Tintoretto, Castrette di Villorba, Italy, 2006.

[69] T. Oey, A. Kumar, J.W. Bullard, N. Neithalath, G. Sant, The filler effect: The influence of filler content and surface area on cementitious reaction rates, J. Am. Ceram. Soc. 96 (2013) 1978–1990. doi:10.1111/jace.12264.

[70] J. Vera-Agullo, V. Chozas-Ligero, D. Portillo-Rico, M. García-Casas, A. Gutiérrez-Martínez, J. Mieres-Royo, J. Grávalos-Moreno, Mortar and Concrete Reinforced with Nanomaterials, in: Z. Bittnar, P. Bartos, J. Němeček, V. Šmilauer, J. Zeman (Eds.), Nanotechnol. Constr. 3, Springer, Berlin, Heidelberg, 2009: pp. 383–388. doi:10.1007/978-3-642-00980-8_52.

[71] H. Moosberg-Bustnes, B. Lagerblad, E. Forssberg, The function of fillers in concrete, Mater. Struct. 37 (2004) 74–81. doi:10.1617/13694.

[72] E. Berodier, K. Scrivener, Understanding the filler effect on the nucleation and growth of C-S-H, J. Am. Ceram. Soc. 97 (2014) 3764–3773. doi:10.1111/jace.13177.

[73] R.T. Yang, Gas Separation by Adsorption Processes, Butterworth Publishers, Stoneham, 1987.

[74] M. Gonçalves, M. Molina-Sabio, F. Rodriguez-Reinoso, Modification of activated carbon

hydrophobicity by pyrolysis of propene, J. Anal. Appl. Pyrolysis. 89 (2010) 17–21. doi:10.1016/j.jaap.2010.04.009.

[75] S. Ranjan, D. Nandita, E. Lichtfouse, Nanoscience in Food and Agriculture 1, Springer Nature, 2016. doi:10.1007/978-3-319-39303-2.

[76] M. Zhang, Y. Ma, Y. Zhu, J. Che, Y. Xiao, Two-dimensional transparent hydrophobic coating based on liquid-phase exfoliated graphene fluoride, Carbon N. Y. 63 (2013) 149–156. doi:10.1016/j.carbon.2013.06.066.

[77] S.G. Prolongo, R. Moriche, A. Jiménez-Suárez, M. Sánchez, A. Ureña, Advantages and disadvantages of the addition of graphene nanoplatelets to epoxy resins, Eur. Polym. J. 61 (2014) 206–214. doi:10.1016/j.eurpolymj.2014.09.022.

[78] Y. Benachour, C.A. Davy, F. Skoczylas, H. Houari, Effect of a high calcite filler addition upon microstructural, mechanical, shrinkage and transport properties of a mortar, Cem. Concr. Res. 38 (2008) 727–736. doi:10.1016/j.cemconres.2008.02.007.

[79] S. Monosi, D. Sani, F. Tittarelli, Used Foundry Sand in Cement Mortars and Concrete Production, Open Waste Manag. J. 3 (2010) 18–25. doi:10.2174/1876400201003010018.

[80] F. Çeçen, A. Özgür, Activated carbon for water and wastewater treatment: Integration of adsorption and biological treatment, John Wiley & Sons, 2011.

[81] K.J. Lee, J. Miyawaki, N. Shiratori, S.H. Yoon, J. Jang, Toward an effective adsorbent for polar pollutants: Formaldehyde adsorption by activated carbon, J. Hazard. Mater. 260 (2013) 82–88. doi:10.1016/j.jhazmat.2013.04.049.

[82] A.H. Mamaghani, F. Haghighat, C.-S. Lee, Photocatalytic oxidation technology for indoor environment air purification: The state-of-the-art, Appl. Catal. B Environ. 203 (2017) 247–269. doi:10.1016/j.apcatb.2016.10.037.

[83] C. Giosuè, M. Pierpaoli, A. Mobili, M.L. Ruello, F. Tittarelli, Multifunctional Lightweight Mortars for Indoor Applications to Improve Comfort and Health of Occupants : Thermal Properties and Photocatalytic Efficiency, Front. Mater. 7 (2020) 1–10.

doi:10.3389/fmats.2020.00255.

[84] V. Georgakilas, M. Otyepka, A.B. Bourlinos, V. Chandra, N. Kim, K.C. Kemp, P. Hobza, R. Zboril, K.S. Kim, Functionalization of graphene: Covalent and non-covalent approaches, derivatives and applications, Chem. Rev. 112 (2012) 6156–6214. doi:10.1021/cr3000412.

[85] H. Zhang, X. Lv, Y. Li, Y. Wang, J. Li, P25- graphene composite as a high performance photocatalyst, ACS Nano. 4 (2009) 380–386. doi:10.1021/nn901221k.

[86] X.-Y. Zhang, Graphene/TiO2 nanocomposites: synthesis, characterization and application in hydrogen evolution from water photocatalytic splitting, J. Mater. Chem. 20 (2010) 2801–2806. doi:10.1039/b917240h.

[87] D. Enea, G.L. Guerrini, Photocatalytic Properties of Cement-Based Plasters and Paints Containing Mineral Pigments, Transp. Res. Rec. J. Transp. Res. Board. (2010) pp 52--60. doi:10.3141/2141-10.

[88] W.. Daoud, Self-Cleaning Materials and Surfaces: A Nanotechnology Approach, John Wiley & Sons, 2013. doi:10.1002/9781118652336.

[89] J. Chen, C. Poon, Photocatalytic activity of titanium dioxide modified concrete materials – Influence of utilizing recycled glass cullets as aggregates, J. Environ. Manage. 90 (2009) 3436–3442. doi:10.1016/j.jenvman.2009.05.029.

[90] A. Al-Dahawi, O. Öztürk, F. Emami, G. Yildirim, M. Şahmaran, Effect of mixing methods on the electrical properties of cementitious composites incorporating different carbon-based materials, Constr. Build. Mater. 104 (2016) 160–168. doi:10.1016/j.conbuildmat.2015.12.072.

[91] A. Belli, A. Mobili, T. Bellezze, F. Tittarelli, P.B. Cachim, Piezoresistive behavior of mortars loaded with graphene and carbon fibers for the development of self-sensing composites, in: Adv. Trends Eng. Sci. Technol. III- Proc. 3rd Int. Conf. Eng. Sci. Technol., Taylor & Francis Group, 2019: pp. 37–42.

[92] D.D.L. Chung, Dispersion of Short Fibers in Cement, J. Mater. Civ. Eng. 17 (2005) 379–383.

doi:10.1061/(ASCE)0899-1561(2005)17:4(379).

[93] A. Samková, P. Kulhavý, M. Pechočiaková, Possibilities to improve electromagnetic shielding of plaster composites adding carbon fibers, IOP Conf. Ser. Mater. Sci. Eng. 254 (2017) 042025. doi:10.1088/1757-899X/254/4/042025.

[94] X. Lv, Y. Duan, G. Chen, Electromagnetic wave absorption properties of cement-based composites filled with graphene nano-platelets and hollow glass microspheres, Constr. Build. Mater. 162 (2018) 280–285. doi:10.1016/j.conbuildmat.2017.12.047.

[95] A.P. Singh, M. Mishra, A. Chandra, S.K. Dhawan, Graphene oxide/ferrofluid/cement composites for electromagnetic interference shielding application, Nanotechnology. 22 (2011) 465701. doi:10.1088/0957-4484/22/46/465701.

[96] A. Mahmood, R. Arsalan, M. Zeeshan, Pyrolytic carbonaceous reinforcements for enhanced electromagnetic and fracture response of cementitious composites, J. Clean. Prod. 248 (2020) 119288. doi:10.1016/j.jclepro.2019.119288.